The Design and Operation of a CAMAC Based Data Acquisition System for the Narodny Ion Accelerator and the Calibration of a NE-102 Plastic Scintillator Neutron Detector Using Gamma Rays, Monte Carlo Simulation, and an Americium-Beryllium Neutron Source.

By

Hamish L. Johnston

A Thesis Submitted to the Faculty of Graduate Studies

in Partial Fulfilment of the Requirements for the Degree of

Master of Science

Department of Physics

University of Manitoba

Winnipeg Manitoba

ISBN 0-315-77922-5

THE DESIGN AND OPERATION OF A CAMAC BASED DATA ACQUISITION SYSTEM FOR THE NARODNY ION ACCELERATOR AND THE CALIBRATION OF A NE-102 PLASTIC SCINTILLATOR NEUTRON DETECTOR USING GAMMA RAYS, MONTE CARLO SIMULATION, AND AN AMERICIUM-BERYLLIUM NEUTRON SOURCE

BY

HAMISH L. JOHNSTON

A Thesis submitted to the Faculty of Graduate Studies of the University of Manitoba in partial fulfillment of the requirements for the degree of

MASTER OF SCIENCE

Abstract

This thesis consists of two parts. In Part I the design and operation of a personal computer controlled CAMAC data acquisition system is discussed. The data acquisition system was designed to monitor nuclear processes that may occur during the implantation of metals (palladium and titanium) with 60 keV deuterons using the Narodny Ion Accelerator. The data acquisition system was capable of monitoring x-ray production, fast neutron production and the beam current of the Narodny accelerator. The deuterium implantation experiment is also briefly discussed.

Part II of this thesis is an investigation of the neutron detection capabilities of the online neutron monitor (ONM), one of the neutron detectors used in the deuterium implantation exercise. The ONM is a plastic scintillator device which detects neutrons mostly through recoil protons from neutron-proton elastic scattering. The light output response of the ONM was first calibrated in terms of electron equivalent energy units (MeVee) via a Compton scattering experiment. This calibration in electron units is then related to proton energy using a standard parametrization. A Monte Carlo code was used to simulate all significant neutron detection interactions in the scintillator. The Monte Carlo generated light output spectra and calculated the detector efficiency for various neutron energy groups. To test the applicability of the Monte Carlo, the ONM was exposed to neutrons of

determined energy from an americium-beryllium (Am-Be) neutron source. The actual neutron energy was deduced from the neutron time of flight. The time of flight was measured with a technique which employs the detection of the 4.44 MeV gamma ray which may be emitted simultaneously with the neutron. Finally, ONM data obtained during the August 1990 deuterium implantation experimental program is analyzed for evidence of fast neutron and thermal neutron production.

DEDICATION

This work is dedicated to Andrea, whose love and patience I am grateful for.

ACKNOWLEDGEMENTS

The author wishes to express sincere gratitude to a number of individuals whose support was crucial to the success of this project. I thank the entire warm fusion group for their hard work and determination. I thank Fawzi Ikraiam, John Mayer and Phil Unger for welcoming me wholeheartedly to room 601 and for making my stay a pleasant one. I thank Keith Furutani and John Mayer for their assistance in hardware and software development. I thank Dr. Jim Birchall for providing the Monte Carlo code and for his advice on running it. I thank Guy Durocher for his technical support on the Vax cluster. I thank Gilles Roy for the loan of equipment and for sharing both his wisdom and his technical expertise. Finally, I wish to thank Dr. Gary Smith for his patience and encouragement at times when all seemed so bleak.

TABLE OF CONTENTS

	Page
ABSTRACT	ii
DEDICATION	iv
ACKNOWLEDGEMENTS	iv
PART I	1
The Development of a Computer Controlled Data Acquisition System for the Narodny Ion Accelerator and the Application of the System to the Detection of Fast Neutrons During Deuteron Implantation Experiments	
Introduction	2
1. The Ion Implantation Exercise and the COLLECT Data Acquisition System	5
1.1 Introduction	5
1.2 Deuterium Implantation Experimental Procedure	7
1.3 The Data Acquisition Exercise	10
1.4 PC Software	19

PART II 21

A Study of the Online Neutron Monitor Response to Fast Neutrons

Introduction 22

2. Light Output Calibration of the Online Neutron Monitor Using Compton Electrons 30

2.1 Introduction 30

2.2 The Compton Scattering Technique 31

2.3 A Simple Method of Monitoring the ONM Gain 40

3. The Monte Carlo Calculation 45

3.1 Introduction 45

3.2 Light Producing Neutron Interactions 46

3.3 Monte Carlo Input Parameters 50

3.4 Monte Carlo Output 53

4. Exposure of the Online Neutron Monitor to Neutrons of Known Energy 59

4.1 Introduction 59

4.2 The Americium-Beryllium Fast Neutron Source 60

4.3 The Time of Flight Experimental Arrangement 64

4.4 The Time of Flight Data Acquisition System 68

4.5 The Data Acquisition Process 72

4.6 Results and Analysis 73

4.6.1 The Time of Flight Spectrum 73

4.6.2 The Neutron Energy Spectrum 76

4.6.3 The Online Neutron Monitor Spectra 80

4.6.4 Comparison With Monte Carlo Predictions 83

4.7 Discussion 88

4.8 Recommendations for the Improvement of the ONM 94

5. Analysis of Deuterium Implantation Data 99

5.1 Introduction 99

5.2 The August 1990 Data 99

5.3 Online Neutron Monitor Calibration 103

5.4 Identification of the Anomalous Structure Present in the August 1990 Data 106

5.5 Conclusions 117

Appendix 119

Introduction 120

A.1 The COLLECT Data Acquisition Program 120

A.2 The TOF Data Acquisition Program 127

References 132

PART I

The Development of a Computer Controlled Data Acquisition System for the Narodny Ion Accelerator and the Application of the System to the Detection of Fast Neutrons During Deuteron Implantation Experiments

INTRODUCTION

During the late 1970's and early 1980's the cyclotron facility at the University of Manitoba employed a VAX 750 computer system which was used for data acquisition through a CAMAC system and for computational purposes. The Vax 750 was eventually sold and replaced by a department wide network of VAXstation 3100 computers which are currently used for computational purposes only. Since the sale of the VAX 750 computer there has been considerable interest in the development of an alternate data acquisition system which could utilize the CAMAC hardware available at the cyclotron facility. A PC based configuration was chosen because a portable system which could be moved between the cyclotron facility and the Narodny ion accelerator was desired.

The first prototype system to be built at Manitoba was a photomultiplier tube test station. This facility was built to test and calibrate tubes destined for use in the ZEUS calorimeter at the DESY facility in Hamburg Germany (ZE86). Although functional, this facility was never used because duplicate systems in Hamburg and Tokyo were able to handle the task.

The second prototype to be developed is a data acquisition system which is capable of monitoring nuclear processes which may occur during ion implantation

by the Narodny ion accelerator. The first version of that system is described briefly by Durocher et al (DU89).

In this investigation 60 keV deuterons were implanted into metal samples (Palladium and Indium) and the target chamber was monitored for the production of fast neutrons. The data acquisition system performed the following tasks:

1) Signals from a plastic scintillation neutron detector (the online neutron monitor or ONM) were digitized and stored in the computer.

2) The beam current of the ion accelerator was monitored in real time.

3) The real time of the experiment was monitored such that the time at which each ONM event occurred was recorded.

4) The rate at which the ONM was detecting events was recorded. This rate is in general greater than the rate at which ONM events are digitized because of the dead time of the system.

In the summer of 1990 this system was modified and these changes are described briefly by McKee et al (MC91). The 1990 system was similar to the original system with the addition of a high purity germanium x-ray detector and

associated electronics, a modification of the beam current monitoring technique and the data acquisition computer code. Part I of this work describes in detail the nature of the ion implantation exercise and the development of the new data acquisition system.

In Part II of this thesis the NIM and CAMAC instrumentation is applied to the task of understanding the response of the online neutron monitor to both neutrons and gamma rays. The purpose of this investigation was to understand the various processes which may contribute to the performance of the ONM as a monitor of the continuous production of neutrons expected during the deuterium implantation process.

CHAPTER ONE

The Ion Implantation Exercise and the COLLECT Data Acquisition System

1.1 INTRODUCTION

The investigations carried out at the University of Manitoba involved the implantation of palladium and titanium metal with 60 keV deuterons using the Narodny ion accelerator (DU89,MC91). During the implantation process the samples were monitored for neutron and x-ray production.

It is well known that many metals including palladium and titanium have the ability to absorb large quantities of hydrogen or deuterium gas. In the Manitoba experiment, metal samples were exposed to a beam of 60 keV deuterons for periods of up to 24 hours. It is believed that during this implantation process significant amounts of deuterium build up within the metal target. These deuterons may act as a target for subsequent deuterons and some deuteron-deuteron fusion is expected (YE89). Fusion reactions involving the collision of an energetic deuteron with a deuteron in the metal lattice are identified as 'warm fusion' processes whereas fusion reactions in which both deuterons have only thermal

energy are identified as 'cold fusion processes'.

The two dominant fusion reaction channels which may occur during the implantation process are as follows (GA89):

$$d + d \rightarrow {}^{3}He\ (0.817\ MeV) + n\ (2.452\ MeV) \qquad \text{Reaction 1-1}$$

$$d + d \rightarrow T\ (1.008\ MeV) + p\ (3.025\ MeV) \qquad \text{Reaction 1-2}$$

Both reactions 1-1 and 1-2 are expected to occur at about the same rate within the metal target. If the fusion products from the above reactions are in abundant supply the following neutron producing reaction is possible:

$$T + d \rightarrow {}^{4}He\ (3.5\ MeV) + n\ (14.1\ MeV) \qquad \text{Reaction 1-3}$$

Several gamma ray producing reactions are of interest because the online neutron monitor is also an efficient detector of gamma radiation:

$$d + d \rightarrow {}^{4}He + \gamma\ (23.8)\ MeV \qquad \text{Reaction 1-4}$$

$$d + p \rightarrow {}^{3}He + \gamma\ (5.488\ MeV) \qquad \text{Reaction 1-5}$$

Reaction 1-4 is expected to be about 4 or 5 orders of magnitude less probable than reactions 1-1 and 1-2.

1.2 DEUTERIUM IMPLANTATION EXPERIMENTAL PROCEDURE

The Narodny ion accelerator (NIA) is a simple linear accelerator capable of accelerating singly charged ions up to an energy of approximately 120 keV (see figure 1-1). Ions are produced in a duoplasmatron type ion source located at the top of the assembly. The ions are extracted from the source, focused by a magnetic lens, and then accelerated down a column of parallel plates which drop in voltage and provide a uniform accelerating electric field. The beam is then guided by electric deflection plates to the beam cube located near the floor. The whole system is maintained in a near vacuum environment by a diffusion pump-coldtrap vacuum system.

The metal samples are placed on a copper sample holder in the sample chamber. The sample chamber is an aluminium cube with a kapton window on one side face to allow for the passage of x-rays to the HPGe x-ray detector. The sample holder is electrically isolated from the rest of the accelerator. The number of ions that strike the target is determined by measuring the current which flows between the sample holder and ground.

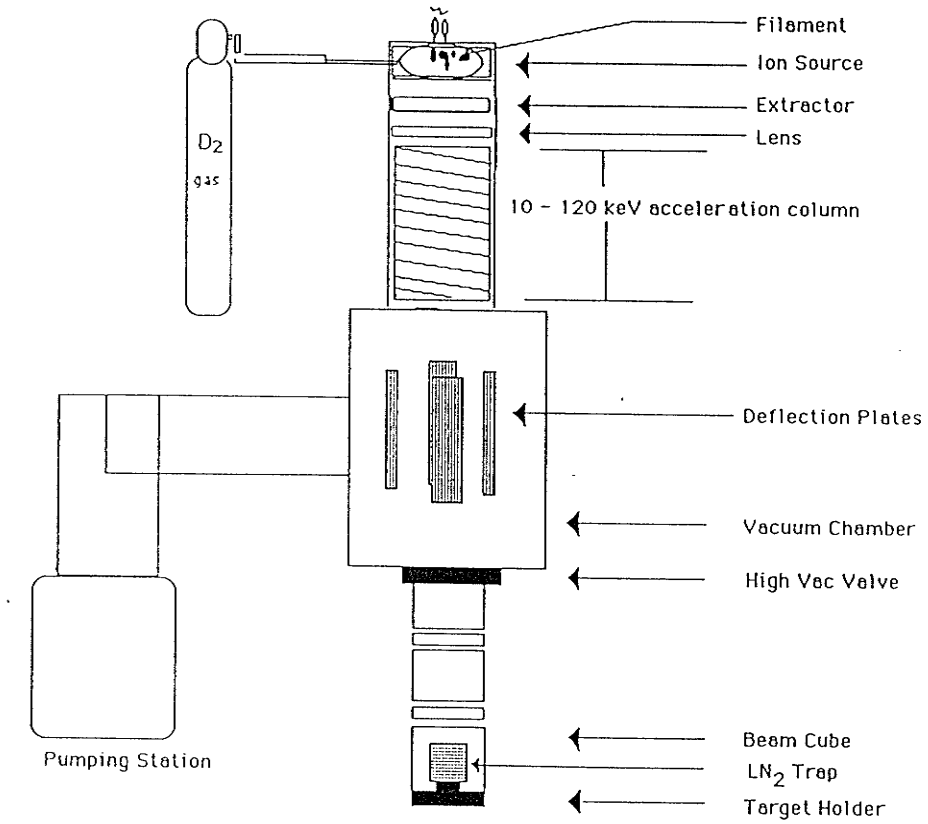

Figure 1-1

The Narodny Ion Accelerator.

Neutron production is monitored in two ways. A piece of indium metal (In) is placed between the metal sample and the copper sample holder. The In is activated by fast neutrons into an excited metastable state with a half life of 4.58 hours. The indium decays back to the ground state by emitting a distinct 331 keV gamma ray.

After the implantation process is completed the indium is removed from the sample chamber and placed near a sodium iodide counter. A spectrum is taken every hour until the gamma ray peak vanishes. Using the reaction cross-section for neutrons of approximately 2 MeV and the gamma ray spectra, the total number of neutrons incident on the indium during the implantation process may be estimated. A detailed description of this measurement is given by Yeo (YE89). Neutron production was also monitored by the online neutron monitor (ONM) which will be discussed in detail in the following chapters.

During the deuterium implantation the HPGe detector viewed the sample through an x-ray transparent kapton window at a distance of 15 cm. The ONM neutron detector was placed 1 metre from the sample. The ONM was placed on the lower shelf of a metal framed cart. The ONM was placed within the cart because it was discovered that the ONM is very sensitive to environmental magnetic fields. The ONM seemed to operate best in the vicinity of the cart which consisted of many closed loops of steel which may have acted to modify the local

magnetic fields.

1.3 THE DATA ACQUISITION SYSTEM

Introduction:

To monitor all interesting facets of the ion implantation experiment a fully automated, computer controlled data collection system is essential. The ion implantation process is a non-equilibrium one, and therefore it is essential to be able to monitor the sample on a real time basis, recording each individual ONM or HPGe event as well as the time at which the event occurred and the accelerator beam current at that time.

The CAMAC computer interface system was chosen because of the availability of CAMAC components at the cyclotron facility. Most of these components were originally used in nuclear physics experiments at the cyclotron facility and thus are ideally suited to process signals from the ONM photomultiplier tubes and the HPGe x-ray detector. The data acquisition system is controlled by a PC computer which is interfaced to a CAMAC crate. Data is collected by the PC and stored on the PC hard disk. When the hard disk becomes full, the operator must manually dump the data onto one of the computers in the VAX cluster.

The data acquisition system performed the following tasks during the ion implantation exercise:

Real Time Monitoring:

In an experiment of the type dicussed it is important to determine the time at which an x-ray or neutron event occurred. A 60 Hz Canberra 807 pulser provides a time base for the system. The pulser is fed into the CAMAC scalar which is read regularly by the PC as part of the data collection process.

Beam Current Monitoring:

Also of importance is the rate at which deuterons strike the target material. The beam current is monitored by a BIC 1000 current integrator. This device is connected between the target holder and ground. As the positively charged deuterons enter the target, current must flow to ground to maintain electrical neutrality. The BIC 1000 integrates this current by charging up a capacitor and emitting a pulse once a certain amount of charge has accumulated. The pulses are counted in the CAMAC scalar. The scalar count at a given time is proportional to the total amount of charge deposited on the target. During a normal implantation run some of the beam strikes the sample holder and thus the charge deposited on the actual sample will be less than the total charge deposited.

When a deuteron strikes the sample it is possible that electrons may be liberated from the sample and accelerated up the Narodny column. If electrons are removed from the sample, an increase in the current between the sample and ground would be required to maintain the electrical neutrality of the sample. Therefore, if electrons are being liberated during the implantation process it is possible that the current measured between the sample and ground is greater than the actual accelerator beam current.

The X-ray Detection System:

An ORTEC HPGe (Hyper Pure Germanium) solid state detector is used to monitor x-ray production in the energy range from about 8 to 100 keV. The HPGe requires a biasing voltage of -1000 V which is provided by a voltage supply mounted in the electronics rack. The HPGe also has a built in pre-amp which is powered by a supply located in the Narodny room, near the detector. Figure 1-2 provides a schematic representation of the HPGe detection electronics.

The signal from the HPGe is sent to the electronics rack via an RG 58 cable. The signal is first amplified by an Ortec 472A spectroscopy amplifier which provides a shaped positive pulse of up to 8 volts. At this point the amplified signal is split in order to gain information regarding the dead time of the detection system.

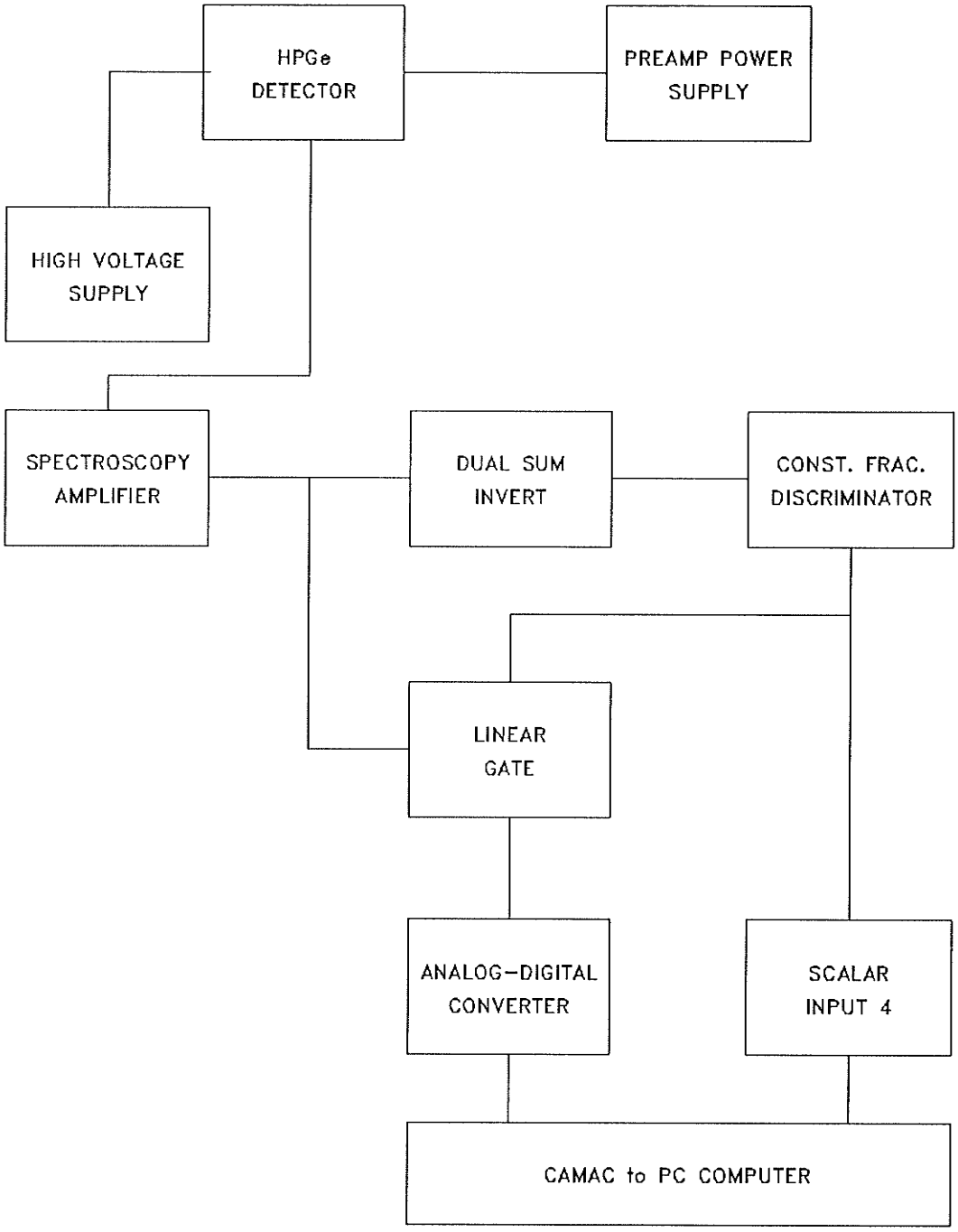

FIGURE 1-2

Hyper pure germanium
x-ray detector electronics.

One branch of the signal is inverted by a dual sum and invert amplifier and fed into a constant fraction discriminator. The signal is inverted because the discriminator only accepts negative signals. The discriminator provides a gate pulse to a linear gate as well as a logic pulse to the 3610 scalar. The discriminator generates a gate pulse only when it receives a signal from the HPGe above 0.2 V., thus the scalar will record the number of events detected by the HPGe above this threshold.

The second branch takes the signal to a linear gate. The linear gate will pass the signal only if it has received a gate pulse from the discriminator. If a gate pulse is received the signal is passed to a Lecroy 3511 ADC where it is digitized and the numerical data is passed to the PC via the CAMAC system.

The number registered by the scalar represents the total number of signal pulses directed at the ADC. In the ideal situation the ADC should digitize all these pulses but in practice it cannot. If we compare the number of pulses digitized to the number registered by the scalar we may estimate the dead time of the x-ray detection system.

The Online Neutron Monitor:

The online neutron monitor (ONM) is a coincidence type unit which is designed

to detect the interaction of neutrons with a piece of plastic scintillator. Such interactions may include neutron-proton elastic scattering, neutron-carbon elastic and inelastic scattering and many other processes which will be described in detail in part two of this work. The ONM consists of a cylindrical piece of NE-102 scintillator optically coupled at the flat ends to two RCA 4522 photomultiplier tubes. The entire assembly is wrapped in black electrical tape to ensure that environmental light does not leak into the sensitive volume.

The predominant detection mode for fast neutrons is neutron-proton elastic scattering. If a neutron collides with a proton in the NE-102 the proton will recoil and may have gained significant kinetic energy. As the proton travels through the NE-102 it will quickly lose energy, predominantly through interacting with electrons. In this process light is given off. Part of this light will be collected by the two photomultiplier tubes which then convert the light into an electrical pulse. When a neutron interacts in the NE-102 scintillation light should be detected by both photomultiplier tubes, and thus a pulse from both tubes is required before an event is registered. A coincidence discrimination circuit has been constructed to ensure that this criterium is met. A schematic diagram of the electronics associated with the ONM is presented in figure 1-3.

The signal from each tube is split into two signals. Two channels of a Lecroy 821 leading edge type discriminator are used to provide a logic timing pulse from

FIGURE 1–3

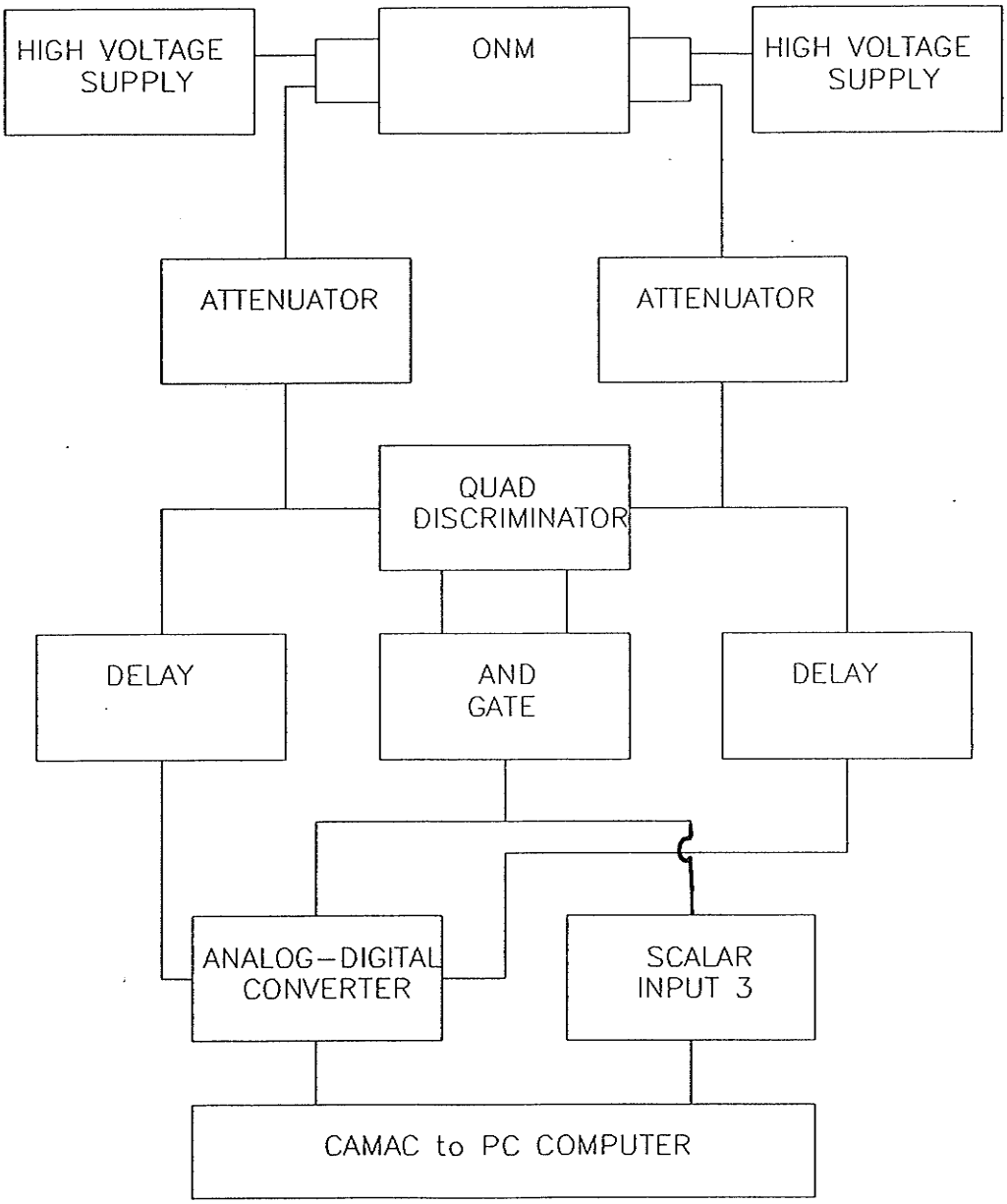

Online neutron monitor (ONM) electronics.

each tube. Both timing pulses are five nanoseconds wide. The timing pulses are fed into a Lecroy 365AL logical AND gate which provides a gate pulse if the timing pulses overlap for at least one nanosecond. This coincidence requirement virtually eliminates any random events due to photomultiplier tube noise. The coincidence requirement also acts as a lower level discriminator, requiring that a valid event must produce sufficient light to fire both lower level discriminator channels.

A 50 ns wide gate pulse is generated by the AND gate and is used to gate the Lecroy 2249A ADC which separately digitizes the signals from both tubes. Because the discrimination processes take approximately 32 nanoseconds the tube signals must be delayed accordingly before they reach the ADC. The digitized information is then sent to the PC via the CAMAC system.

If a large amount of energy is deposited in the ONM, one or both of the 2249A ADC channels may overflow. If this occurs the data will still be digitized, yielding a distinct overflow value and the data files are later purged of these events. This acts as an effective upper level discriminator which will eliminate very large pulses.

A pulse height spectrum of the ONM is constructed by summing the ADC values from each of the photomultiplier tubes to obtain a total light output for each valid event. Because of the summing procedure and the coincidence requirements it is important to ensure that both channels are operating with the same gain. This

is accomplished by viewing the output of each tube separately over a wide range of pulse heights and fine tuning the photomultiplier tube gains until both tubes appear to be behaving similarly.

The AND gate also provides a pulse to the 3610 scalar. This provides a record of how many signal pulses are sent to the ONM ADC. The ADC is not capable of processing all the pulses and so the information stored in the scalar allows us to estimate the dead time of the ONM.

A summary of data stored by the 3610 scalar is presented below, the number corresponds to the scalar channel.

1) Beam current from current integrator
2) Time from 60 Hz pulse
3) ONM coincidence from AND gate
4) HPGe events from const. frac. disc.
5) 3511 ADC busy out
6) Not used

1.4 PC SOFTWARE

The data acquisition process is controlled by the PASCAL program COLLECT. Details regarding the CAMAC hardware and software interface and a complete listing of the COLLECT source code are provided in the appendix to this work.

The COLLECT program is simply an infinite loop which constantly interrogates the CAMAC system for a look at me (LAM) signal. A LAM is generated by the 3511 ADC or the 2249A ADC after the unit has digitized a pulse and is ready to transfer data along the CAMAC dataway to the PC. If a LAM is detected COLLECT calls the LAMHandler procedure.

The LAMHandler procedure calls the extract_data procedure which tests to see which ADC generated the LAM and then extracts the data from one or both of the ADCs. If an ADC did not assert a LAM the data corresponding to that ADC will be assigned a value of 9999 to ensure that it is identified as a non-event.

The event_builder procedure is then called to format the data. The data is stored in a one dimensional array. 41 sets of ADC data are stored before the data is transferred to the PC hard disk. Each set of data consists of the three numbers generated by the extract_data procedure, one number from the 3511 ADC and two numbers from the 2249A ADC. Once 41 sets of data have been collected the

event_builder procedure reads the 5 channels of the CAMAC scalar and adds these numbers to the end of the one dimensional array. Thus a data set consists of 123 numbers from the ADC's and five numbers from the scalar for a total length of 128. This data array is then transferred to the PC hard disk.

The COLLECT program will continue to fill the PC hard disk with data until the experimenter manually initiates a data dump to the VAX computer. The COLLECT program will then log onto a VAXstation 3100 computer and transfer the data over an ethernet line. This process usually takes a few seconds but may take up to a few minutes if other VAX users are trying to access data on the VAX hard disk used to store the COLLECT data. During the data transfer the COLLECT program is unable to acquire data from the CAMAC system. Thus, the data dump should be initiated during a relatively quiet time in the experiment. Each dump to the VAX computer is stored as a separate subrun with file name RUN#.SUBRUN#.

On the VAX system, the data is stored in large binary files. Fortran codes have been written which decode these files and allow the data to be organized into time intervals selected by the operator. Histograms of the ONM and HPGe may be generated for any particular time interval selected by the operator. The fortran code also calculates the average beam current in each time interval.

PART II

A Study of the Online Neutron Monitor Response To Fast Neutrons

INTRODUCTION

Part II of this work is devoted to the study of the online neutron monitor (ONM) as a detector of fast neutrons. As an introduction to this analysis, a short survey of the theory and practice of organic scintillator neutron detection is presented. It is the author's hope that this brief introduction will serve to stimulate discussion of possible improvements to the present neutron detection system.

FAST NEUTRON DETECTION USING ORGANIC SCINTILLATORS

Shortly after the discovery of organic scintillators it was suggested by Bell that these materials could be used to detect fast neutrons via neutron proton (n-p) collisions (BE48). This discovery and the development of the scintillator-photomultiplier tube technique was responsible for rapid progress in the field of fast neutron physics.

In general, organic scintillators are very useful in the detection of fast neutrons because they contain a large amount of hydrogen and thus provide a medium in which the energy imparted to the proton in an n-p collision can be efficiently converted into scintillation light. Many different types of organic scintillators have been developed. These materials can be grouped into three general categories: Crystalline scintillators, plastic scintillators and liquid scintillators. Crystalline

organic scintillators were the first to be developed and have since fallen from favour because of the inconvenience of working with fragile crystals and the observation that the response of the scintillator was a function of the crystal orientation relative to the incident radiation for heavy particles such as protons. Since the late 1960's plastic and liquid organic scintillators have been used almost exclusively.

NE-102 AS A DETECTOR OF FAST NEUTRONS

The online neutron monitor (ONM) is a right cylinder of NE-102 plastic scintillator viewed at both flat ends by a photomultiplier tube. Although NE-102 is not the ideal detection medium for a low event rate search for MeV neutrons it does have a limited usefulness in this application.

The basic problem with the choice of NE-102 is the effect of gamma radiation on low counting rate neutron detection in the MeV neutron energy region. For example, environmental gamma rays in the 0.500 to 2.0 MeV energy range will produce light signals in the ONM comparable to neutrons in the 1.0 to 5.0 MeV energy range (see chapter 2 for details). With the present ONM it is impossible to discriminate between neutron and gamma ray events and thus the ONM has a rather limited usefulness as a low counting rate fast neutron detector.

PULSE SHAPE DISCRIMINATION

It was observed by Brooks in 1956 that in many organic scintillators the pulse shape due to recoil protons and the pulse shape due to compton electrons (the only significant detection process for MeV gamma rays in an organic scintillator) was different (BR59). A pulse shape discrimination technique has since evolved which uses this difference to discriminate between neutron and gamma ray events.

In all organic scintillators the amplitude of the light pulses will decrease with time. This decay can be described as exponential with a short lifetime of about one nanosecond and a long lifetime of about 100 nanoseconds (HA79). An electron, which deposits relatively little energy per unit path length in the scintillator, tends to excite isolated individual molecules. These molecules deexcite very rapidly to produce a pulse in which the short lifetime dominates. Conversely, the proton deposits a large amount of energy per unit path length and tends to create a path of closely spaced excited molecules. Interactions between these molecules tends to hinder the rapid deexcitation process via competing modes of deexcitation. The result is a pulse with a lifetime much greater than that of an electron (see for example figure 7.12 in Leo) (LE87).

The experimenter can use this difference in decay time to discriminate between neutron and gamma ray events. With the advent of fast current integrating analog

to digital converters a simple approach to pulse shape discrimination would be to separately digitize the fast component of each pulse (the first 50 ns) and the slow component of each pulse (50 to 300 ns) and compare the relative size of the components (see for example the recent work of Filchenkov et al (Fl90)).

Unfortunately, plastic scintillators such as NE-102 are designed for fast timing applications and are formulated to minimize the slow decay processes. As a result NE-102 has very poor pulse shape discrimination properties and is rarely used in this context. Liquid organic scintillators such as NE-213 have been formulated specifically for pulse shape discrimination and have been commercially available for at least 25 years.

THE NEUTRON DETECTION PROPERTIES OF NE-102 COMPARED TO NE-213

NE-102 has been used by many investigators as a relatively efficient detector of fast neutrons. NE-102 has the following desirable qualities with regards to neutron detection:

- NE-102 is composed principally of carbon and hydrogen, both effective in the detection of neutrons (see chapter 3 for a full discussion). The hydrogen to carbon ratio is 1.104.

- NE-102 is a plastic which is physically very durable and easy to machine into any shape that is desired.

- NE-102 has a very fast response time. This allows the coincidence requirement of the ONM photomultiplier tubes to be set very tightly and random false events due to photomultiplier tube noise are virtually eliminated.

NE-213 shares many desirable features with NE-102 except that in being a liquid, NE-213 must be held in some sort of container with a window suitable for the transmission of scintillator light to the photomultiplier tube. Usually, commercially produced NE-213 scintillators are supplied encapsulated in a suitable container.

For low counting rate detection of neutrons or the detection of neutrons in a high gamma ray environment NE-213 is suitable for the following reasons.

- NE-213 has a hydrogen to carbon ratio of 1.213 which is greater than NE-102. This means that the effective Z of NE-213 is less than that of NE-102. Compton scattering of gamma rays increases as Z and thus NE-213 is a less efficient detector of gamma rays than NE-102.

- NE-213 is able to provide a means of discrimination between gamma rays and

neutrons.

It is the opinion of the author that NE-213 would have been a better choice for construction of the ONM. The present ONM electronics could quite easily act as a pulse shape discrimination system with the addition of a delay and another 2249A analog to digital converter. The time of flight method used in chapter 4 could be modified to test and calibrate the pulse shape discrimination properties of the system using the neutrons and gamma rays which emanate from an Am-Be neutron source.

For a general discussion on proton recoil neutron detection using various organic scintillators the reader is directed to the following works; Birks (Bl64) and Knoll (KN89). An excellent review of a number of neutron detection techniques including organic scintillators is presented by Harvey and Hill (HA79). A concise, general discussion of the scintillation process is given in a 1979 review paper by Brooks (BR79).

THE CALIBRATION TECHNIQUE

Before any modifications to the ONM can be made, the present system must be well understood. The remainder of this work is devoted to the investigation of the ONM as a detector of neutrons in the energy region of one to eight MeV. As

a result of this calibration, the response of the ONM to gamma radiation in the energy range of about 0.5 to 1.3 MeV will also be investigated.

The calibration procedure can be summarized in the following steps:

1) The ONM is exposed to several gamma ray sources which results in the detection of compton electrons. Using a coincidence method to select monoenergetic compton electrons, the light output of the ONM is calibrated in units of electron equivalent MeV or MeVee. One MeVee is defined as the light output corresponding to a one MeV stopping electron. The light output of an organic scintillator is a linear function of electron energy which makes this calibration scheme a convenient one.

2) In the energy region of interest the light output of recoil protons is not a linear function of proton energy. An empirical parametrization unique to NE-102 is employed to convert the light output for protons to that of electrons.

3) A Monte Carlo code is employed which predicts the neutron light output spectrum. The output of the Monte Carlo is given in units of MeVee. The calibration of step 1 allows the Monte Carlo spectra to be compared to actual ONM spectra.

4) To confirm the predictions of the compton calibration and the Monte Carlo simulation, a time of flight experiment was performed which subjected the ONM to neutron groups of well defined energy.

5) The results of the investigation will be analyzed and recommendations will be put forth for the improvement of the online neutron monitor.

6) Data from the deuterium implantation experiments of August 1990 will be analyzed.

CHAPTER TWO

Light Output Calibration of the Online Neutron Monitor Using Compton Electrons.

2.1 INTRODUCTION

In the neutron energy region of a few MeV the dominant neutron detection process in an organic scintillator is neutron-proton elastic scattering (n-p). For neutrons with energies of a few MeV the n-p interaction is a non-relativistic 'billiard ball' like collision. If we assume that the proton and neutron have the same masses the n-p collision is symmetric in the centre of mass system. This results in recoil protons with energies ranging from zero to the full energy of the incident neutron (SW60).

The recoil protons are very short ranged in the scintillator and create very dense ionization tracks. It was observed by Birks that the light output of organic scintillators is not a linear function of proton energy for protons of a few MeV (BI51). Birks has suggested that the proton deposits much more energy per unit path length then can be converted into scintillation light. This effect, called quenching, is a result of interactions between neighbouring excited molecules

which results in a significant amount of ionizing energy lost to non-light producing deexcitation modes. It has also been suggested that permanent damage may be inflicted upon the scintillator by heavily ionizing particles. This damage may also contribute to the quenching effect and reduce light output for heavy particles such as protons (BR79).

Electrons in the same energy region have a much longer range in the scintillator and deposit much less energy per unit path length. For electrons, most of the energy loss is due to light producing interactions and as a result the light output of organic scintillators is a linear function of electron energy for energies greater than about 100 keV (BI64).

Because of the nonlinear response of organic scintillators to protons it is standard practice to calibrate the light output of these detectors in units of electron equivalent MeV or MeVee. This unit is defined as the light output corresponding to a stopping one MeV electron.

2.2 THE COMPTON SCATTERING TECHNIQUE

The most convenient method of calibrating the light output of an organic scintillator detector is via a Compton scattering experiment. Because of the relatively low density of organic scintillators, the Compton scattering of electrons

is the only significant mode of interaction for gamma rays. The detector is exposed to a known gamma source. The energy of the Compton electrons may be defined by placing a NaI detector at a specific scattering angle to detect the scattered gamma ray. A coincidence between the ONM and the NaI detector is required before the data from the ONM is digitized.

The Compton method is convenient for two reasons:

1) Through the use of different gamma ray sources and different scattering geometries a wide range of Compton electrons may be selected.

2) Because the incident gamma rays have a mean path length comparable to the thickness of the detector the Compton events will occur in the bulk of the detector. This is desirable because during the neutron detection process most light producing events also occur in the bulk of the detector.

Compton scattering experiments were performed using gamma rays from ^{22}Na ^{137}Cs and ^{60}Co. The scattering geometry was fixed at a scattering angle of 135 degrees. The time of flight system described in Chapter 4 was used to collect data and enforce the coincidence requirement between the NaI detector and the ONM. The electronics and software employed were identical to that used in the time of flight measurement (described in chapter four of this thesis) except that a much

smaller NaI crystal was used to more precisely define the scattering angle. A diagram of the scattering geometry is presented in figure 2-1.

ONM spectra corresponding to the following Compton electrons are shown in figures 2-2(a), 2-2(b) and 2-2(c):

^{22}Na: 0.511 MeV gamma ray yields a 0.322 MeV electron.

1.275 MeV gamma ray yields a 1.037 MeV electron.

^{137}Cs: 0.662 MeV gamma ray yields a 0.456 MeV electron.

^{60}Co: 1.333 MeV gamma ray yields a 1.090 MeV electron.

Figure 2-2(d) shows a plot of electron energy versus ONM channel number. The data presented in figure 2-2(d) fits the following relationship:

$$E(\text{MeVee}) = (A \times \text{CHANNEL}) + B \qquad \text{Equation 2-1}$$

Where E is the electron energy in units of MeV or MeVee, CHANNEL is the ONM channel number and;

$$A = 0.009106 \text{ MeVee/CHANNEL}$$

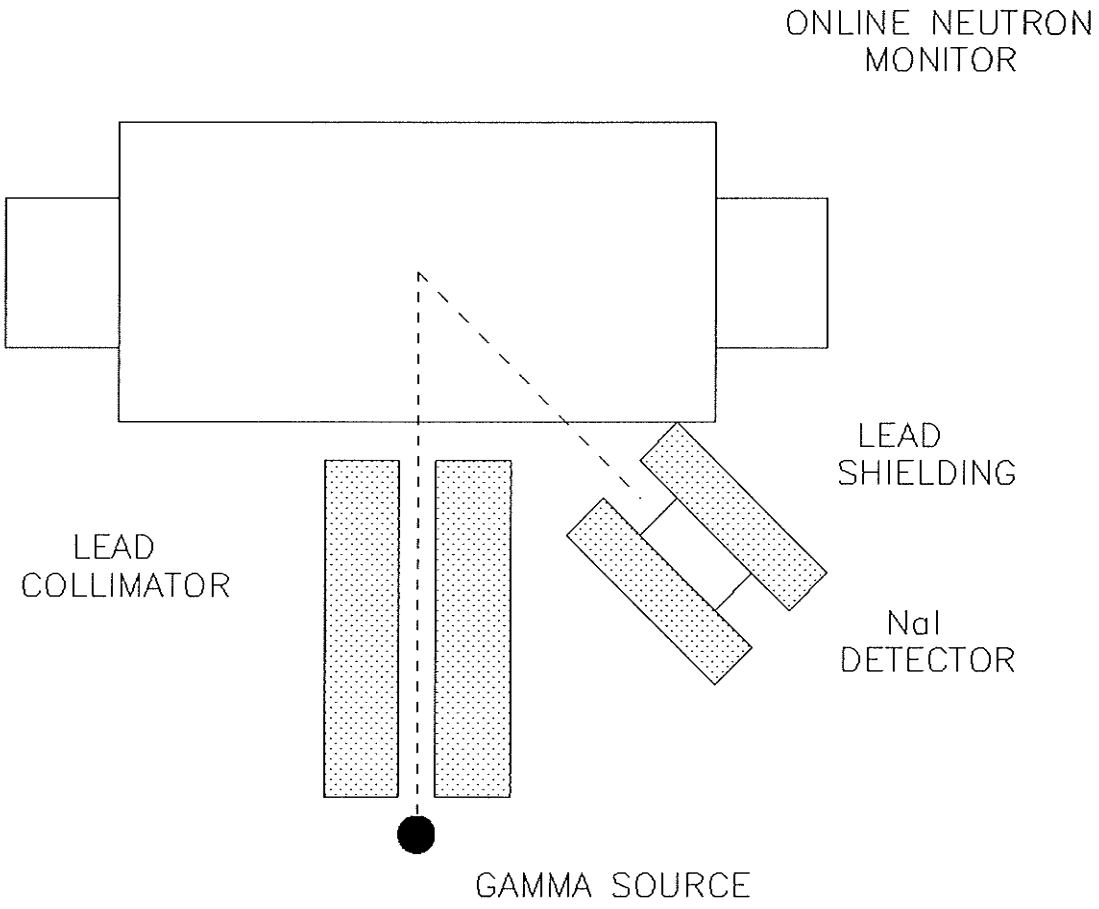

FIGURE 2-1

Compton calibration
experimental arrangement.

Figure 2-2

ONM spectra showing compton electrons corresponding to:

(a) ^{22}Na, (b) ^{137}Cs and (c) ^{60}Co.

(d) Light output calibration of the ONM using the above compton electrons.

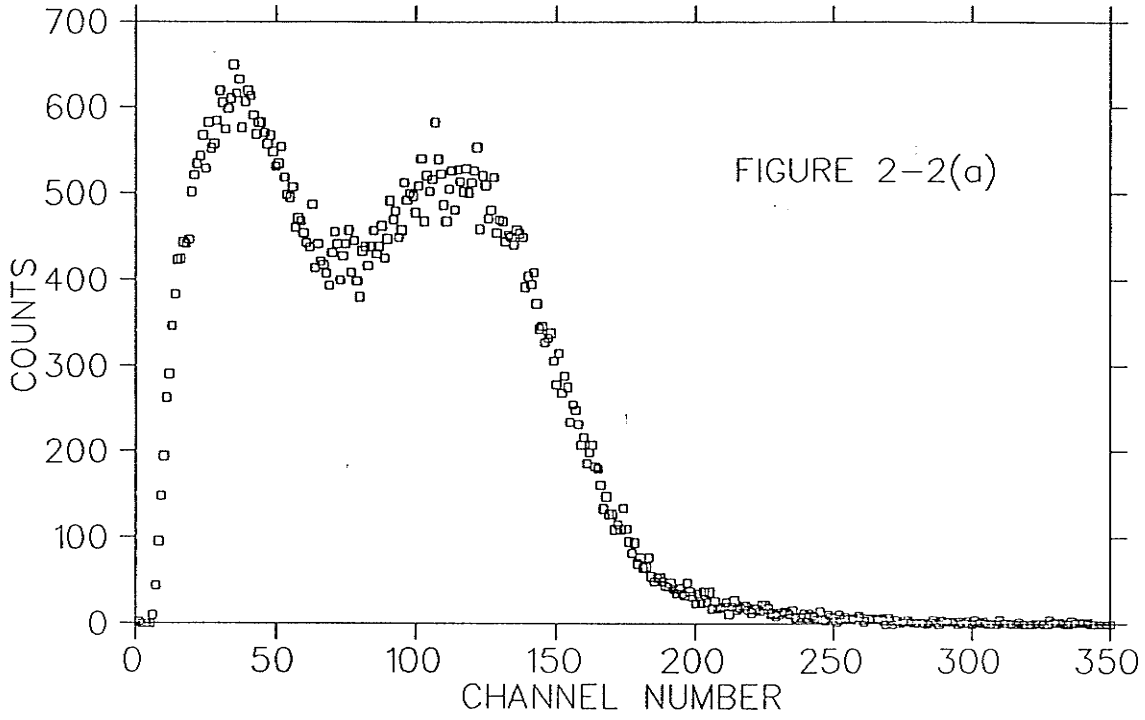

FIGURE 2-2(a)

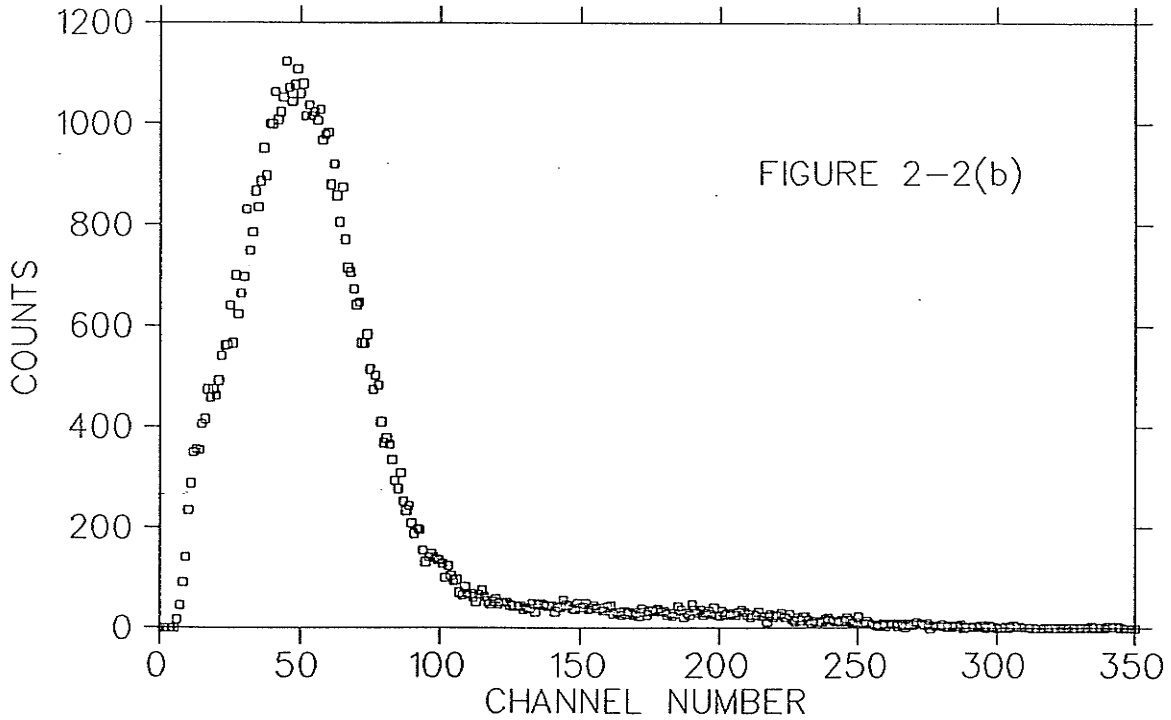

FIGURE 2-2(b)

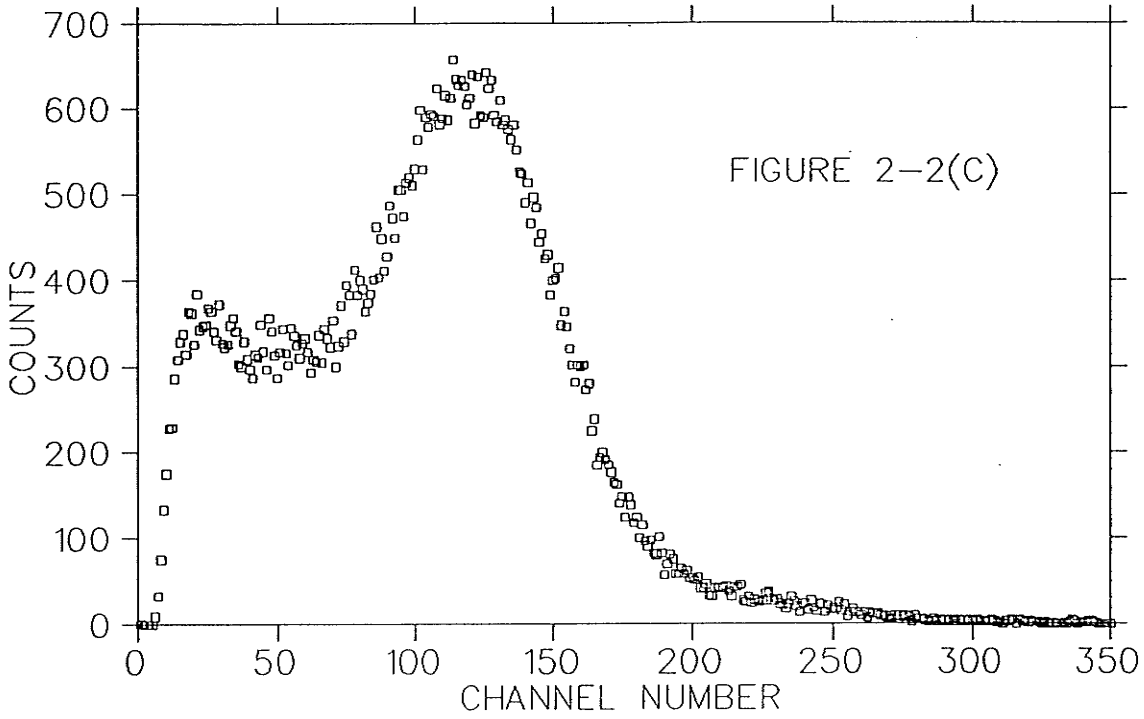

FIGURE 2-2(C)

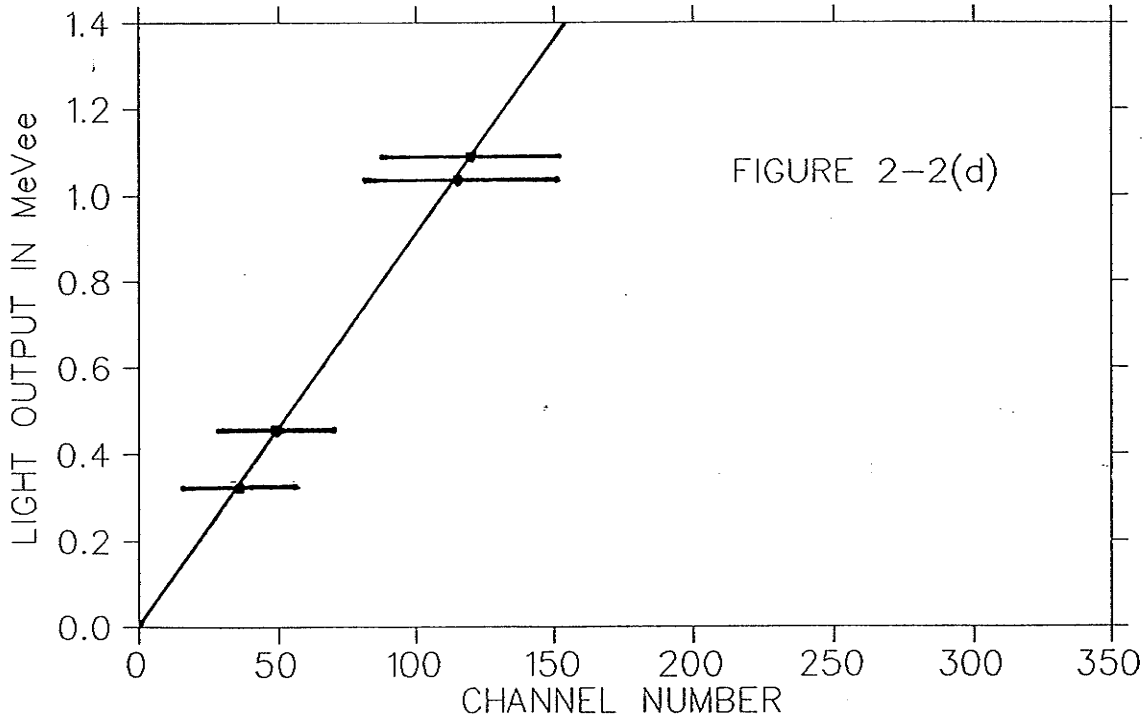

FIGURE 2-2(d)

$B = 0.004950$ MeVee

The next task is to express the above calibration in terms of proton energy. Much effort has been made to compare the light output of protons to electrons in many organic scintillators including NE-102. An excellent review of the relevant literature can be found in the 1970 work of Craun and Smith (CR70).

The definitive work concerning NE-102 is the 1978 work of Madey et al (MA78). In this work the authors fit light output data from three different investigators to an empirical expression. The data ranges over proton energies from 0.25 MeV to 10.5 MeV. Madey suggests the following expression:

$$T_e = A_1[1-\exp(-A_2 T_p^{A_3})] + A_4 T_p \qquad \text{Equation 2-2}$$

Where T_e is the electron equivalent light output for a proton of energy T_p (MeV), and:

$A_1 = -8.0$

$A_2 = -0.10$

$A_3 = 0.90$

$A_4 = 0.95$

The ONM is operated with a bias or lower level discrimination setting of 0.16 MeVee. This corresponds to the same light output as a 0.9 MeV proton. Therefore the detector bias corresponds to a neutron energy of 0.9 MeV. The upper level of the detector is at 2.98 MeVee. This corresponds to the same light output as a 6.7 MeV proton. Thus a realistic upper limit for the ONM is a neutron energy of up to 6.7 MeV. A more detailed analysis of neutron response will be discussed in the following sections of this work.

Note that in the Madey parametrization, the light output T_e assumes a value of zero for a proton energy of about 0.16 MeV. Clearly the parametrization is not applicable at such low proton energies. However, because of quenching effects in the scintillator the proton light output falls off very rapidly with decreasing proton energy. For example, it has been shown by Czirr et al that a 0.25 MeV proton will create as much light as a 0.012 MeV electron (CZ64). This light output is at least one order of magnitude less that the bias of the ONM. Therefore it is reasonable to assume that such low energy protons can essentially be ignored and that a light output of zero for protons of energy 0.16 MeV and less is appropriate.

2.3 A SIMPLE METHOD FOR MONITORING THE ONM GAIN

Although the above method is very effective in calibrating the light output of the ONM in units of MeVee, the coincidence requirement makes this technique cumbersome and time consuming. An alternative calibration technique using the full Compton spectrum of various gamma sources and the cosmic muon spectrum has been developed. This method is recommended as a technique to monitor the ONM response once the coincidence calibration described in the previous section has been performed.

After the ONM was calibrated using the Compton coincidence technique, it was exposed to various gamma ray sources and the full Compton electron spectrum was recorded (no coincidence with another detector was required). The channel corresponding to two thirds of the Compton edge height on the high energy side of each Compton profile was found. Figure 2-3 shows the location of the two thirds channel for ^{137}Cs. Compton profiles from ^{22}Na and ^{60}Co were also used. The following light outputs were assigned to the two thirds positions using equation 2-1.

Gamma Ray Source	Light Output
^{22}Na (0.511 MeV gamma ray only)	0.508 MeVee
^{137}Cs (0.662 MeV gamma ray)	0.565 MeVee
^{60}Co (1.173 and 1.333 MeV gamma rays)	1.290 MeVee

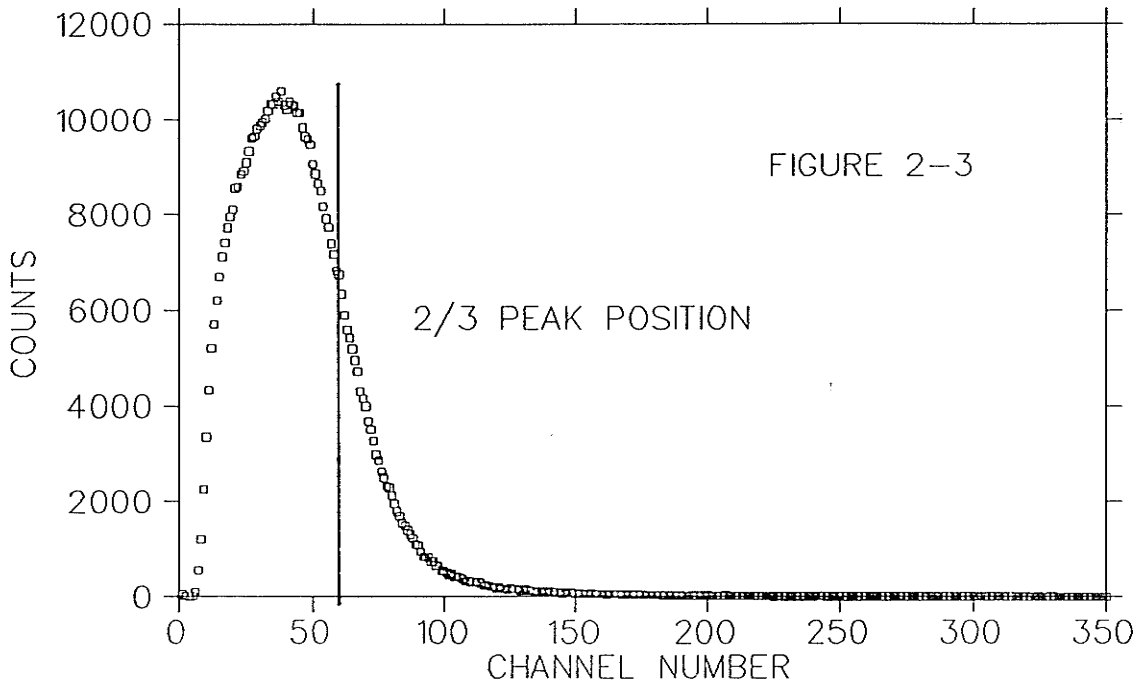

Figure 2-3

Compton profile in the ONM due to the 0.662 MeV gamma ray from ^{137}Cs. The 2/3 peak position discussed in the text is also shown.

Another reference point in the ONM spectrum which may be used for fine tuning the ONM light output calibration is the cosmic muon through peak. In the normal operating mode cosmic muons create large signals in the ONM which usually result in an ADC overflow. To view the full cosmic muon spectrum the signals from the two photomultiplier tubes must each be attenuated using a resistive network to about 20 percent of the original pulse size. The overall effect on the ONM sum spectrum is an effective reduction of gain to 21.7 percent of the original value. This change in gain is measured by observing the shift of a known structure in the ONM spectrum.

The cosmic muon through peak is presented in figure 2-4. A gaussian distribution was fitted to the lower portion of the peak from channel 130 to channel 150. This fit yields a centroid at channel 146 and a standard deviation of 13.0. Correcting for the attenuation in the ONM gain, the cosmic muon through peak is located at channel 674 in the normal operating mode. Using equation 2-1, a light output of 6.14 MeVee is assigned to the cosmic muon through peak. The cosmic muon through peak now provides a high light output reference point for monitoring possible gain fluctuations in the ONM.

With the above information the experimenter has the means to monitor and correct for any shifts in gain which may occur during normal use of the ONM. This method should only be used to fine tune the original coincidence calibration in the

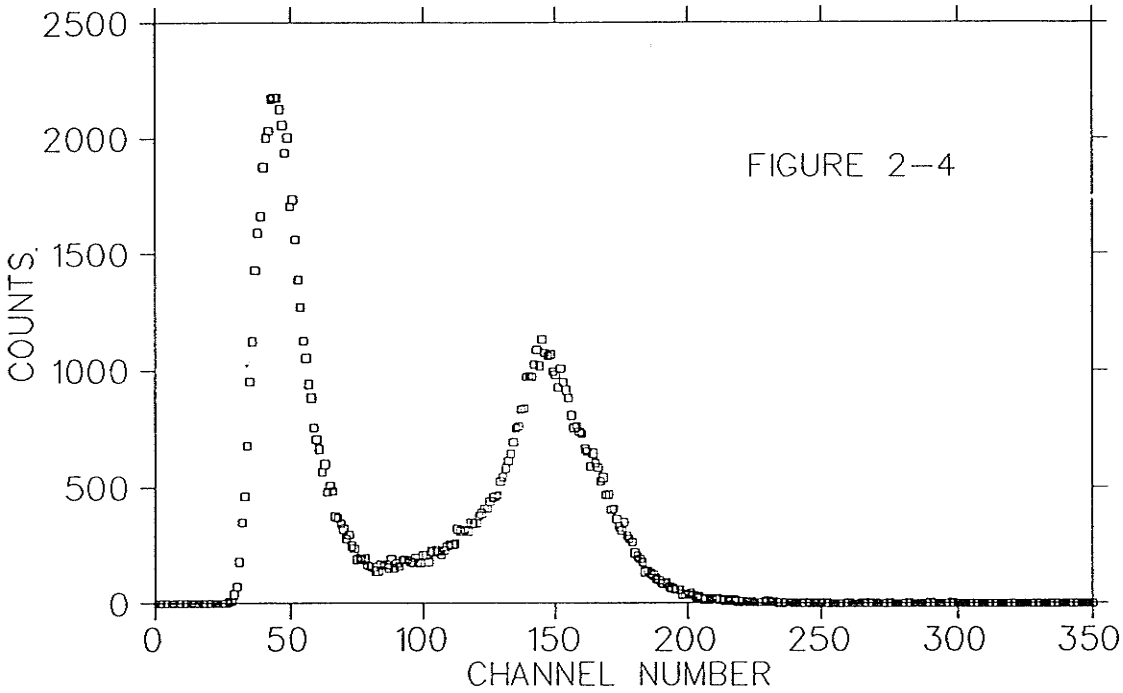

Figure 2-4

ONM spectrum showing the cosmic muon through peak at channel 146. ONM gain is 21.7 percent of the normal operating gain.

event of minor changes to the ONM operating parameters. Such minor changes might include photomultiplier tube gain drift, relocation of the ONM (the ONM response is very sensitive to local magnetic fields) and resetting the system after a power failure. This quick calibration technique also provides a means of checking the ONM response and should be initiated regularly during the operation of the ONM to ensure consistency. If any major changes are made to the operating parameters a full coincidence calibration should be performed. An example of a major change would be the operation of the photomultiplier tubes at new voltage settings or changes to the detector electronics.

CHAPTER THREE

The Monte Carlo Calculation.

3.1 INTRODUCTION

It is very difficult and often impractical to calibrate a neutron spectrometer with a source of real neutrons. Techniques have evolved which attempt to predict both the detection efficiency and scintillation light output spectrum for various detector geometries through the use of computer simulation. The most common technique is the Monte Carlo simulation first developed by Stanton in 1971 (ST71). An improved version of the Stanton code has been used to predict the response of the ONM to neutrons of various energies.

The improved version of the Stanton code has the following desirable features:

1) The neutron is followed through the detector until it escapes or falls below a minimum energy of 0.1 MeV. Therefore all orders of multiple scattering are considered. At 0.1 MeV the neutron is capable of producing very little scintillation light because the recoil protons will be very heavily ionizing (see chapter 2 for details).

2) Scattered protons are monitored and if they escape the scintillator a suitable light output is assigned.

3) The code is adaptable to the geometry of the ONM. The scintillator may be defined as a right cylinder with neutrons incident upon the curved face.

4) The code employs the improved proton light response function postulated by Madey and discussed in the previous chapter.

5) An effort has been made to simulate the effect of the photomultiplier tube photocathode response. This is accomplished by assuming a resolution function which acts to 'smear' the light output (ST71). A one electron level Lo is defined as the light output in MeVee which is required to liberate one photoelectron from the photocathode of the photomultiplier tube. A gaussian distribution is defined from this parameter and is used to randomly smear the light output generated by the Monte Carlo.

3.2 LIGHT PRODUCING INTERACTIONS

To be effective the Monte Carlo code must be able to consider all possible neutron interactions within the scintillator which significantly effect the light output spectrum and the efficiency of the detector. In the energy range of one to eight

MeV seven processes are of interest. Below the carbon inelastic threshold of 4.7 MeV the following elastic processes completely dominate (ST71).

Neutron Proton Elastic Scattering:

This process, which is discussed in detail in chapter 2, is the most significant light production process in the energy range of interest.

Neutron Carbon Elastic Nondiffractive Scattering:

This process is essentially nonrelativistic elastic 'billiard ball' scattering. In the energy range of interest the recoil carbon nucleus is so heavily ionizing that the resulting light production is minimal because of quenching effects in the scintillator. However, this process acts to scatter neutrons and thus has an effect upon the detector efficiency. Stanton claims that for detector geometries similar to the ONM the n-C interaction increases the detector efficiency slightly over that of a pure hydrogen target by scattering neutrons back into the detector (ST71).

Because the carbon nucleus is about twelve times more massive than the neutron, the neutron will only lose between 0 and 28 percent of it's energy in a neutron-carbon collision. If an incident neutron first scatters from a carbon it will still have enough energy to produce a significant amount of scintillation light. In

detectors such as the ONM which have a transverse dimension much greater the depth of the scintillator, a primary scatter from a carbon will actually increase the potential neutron flight path through the scintillator. Therefore the presence of the carbon in the scintillator should tend to increase the efficiency of the ONM and have some effect on the neutron light output spectrum.

If carbon scattered neutrons undergo n-p scattering the resulting pulse height spectrum will be that of neutrons with energies between 72 and 100% of the incident neutron energy. If this spectrum is added to the pulse height spectrum from a pure proton target the resulting spectrum should resemble the pure proton spectrum but with added events in the lower energy region.

At higher incident neutron energies, several other interactions are possible.

Carbon Inelastic Scattering:

The following reaction is possible above 4.7 MeV:

$$n + {}^{12}C \rightarrow n + {}^{12}C + \gamma(4.4\ MeV)$$

In this reaction the carbon nucleus is scattered into the first excited state which

immediately decays to yield a 4.4 MeV gamma ray. The gamma ray may be subsequently detected in the scintillator via compton scattering and contribute scintillation light. The Monte Carlo code has the means to simulate the gamma ray detection. The recoiling carbon will contribute a negligible amount of light.

Near the reaction threshold, the scattered neutron will have very little energy and thus will not have the potential to produce a significant amount of scintillation light. However at higher neutron energies this process serves as a source of scattered, light producing neutrons similar to n-C non diffractive elastic scattering. Stanton claims that the contribution of this reaction to detector efficiency in the energy region of 6 to 16 MeV is less than ten percent of the n-p contribution.

Single Alpha Particle and Beryllium:

The following reaction is possible above 6.2 MeV:

$$n + {}^{12}C \rightarrow \alpha + {}^{9}Be$$

In this reaction both the recoiling alpha particle and the Be nucleus will produce scintillation light but the only significant contribution will be that of the alpha particle. The Monte Carlo code simulates this reaction and calculates a light output corresponding to the alpha particle.

Neutron Carbon Diffractive Elastic Scattering:

The threshold for this process is 7.5 MeV. The angular differential cross section is calculated from the total nonelastic cross section for a given incident neutron energy by the Monte Carlo code.

Three Alpha Particle Production:

The following reaction is possible above 7.9 MeV:

$$n + {}^{12}C \rightarrow n + 3\alpha$$

In this reaction all three alpha particles may contribute to the light production process. The neutron may also go on to another light producing interaction.

3.3 MONTE CARLO INPUT PARAMETERS

The Monte Carlo code requires the following input parameters:

i) Reaction cross sections for all the interactions discussed above. This data was provided by Ramsay (RA91).

ii) Proton and alpha particle light output parameters. The proton parametrization of Madey et al was used. See chapter 2 for a complete discussion of proton light output. The alpha particle parametrization is that of Cecil (CE79) and is of the same form as the Madey parametrization.

iii) The one electron level Lo value. A survey of the literature shows that for a number of different scintillator/photomultiplier configurations investigators use a Lo value on the order of several keVee. For example Cecil, simulating both NE-102 and NE-213 scintillators mounted upon an RCA 7850 photomultiplier tube used an Lo value of 2 keVee (CE79). Ramsay, simulating an NE-213 scintillator mounted upon an RCA 4522 photomultiplier tube used an Lo value of 5 keVee (RA80). Because the Ramsay configuration uses the same photomultiplier tube as the ONM, an Lo value of 5 keVee was chosen for the simulation.

Ramsay claims in his work of 1980 that the choice of Lo is only of crucial importance if the bias setting of the detector is set near the maximum light output. Ramsay also notes that at bias settings less than 50% of the maximum light output the choice of Lo has little effect on the integral efficiency. In the ONM the bias is set at 0.16 MeVee, the maximum light output for a 2.45 MeV neutron is 0.72 MeVee. Therefore, in the case of the ONM the selection of the Lo value is not of crucial importance and the adoption of the Ramsay value is probably sufficient.

iv) The geometry and composition of the detector must be supplied. The ONM is composed of NE-102 with a density of 1.032 g/cm^3 and a hydrogen atom to carbon atom ratio of 1.104. The detector was defined as a right cylinder with a diameter of 13.5 cm and a height of 33.5 cm.

v) The neutrons are selected such that they uniformly illuminate the curved face of the cylinder.

vi) The detector bias is set at zero and the light output spectrum is generated with a bin width of 0.01 MeVee for neutron groups with energies ranging from one to three MeV. For neutron groups with energies ranging from four to eight MeV a bin width of 0.02 MeVee is employed.

vii) The following neutron groups were run:

Neutron Energy	Number of Neutrons
1.00 MeV	30 000
2.00 MeV	30 000
2.45 MeV	30 000
3.00 MeV	30 000
4.00 MeV	40 000
5.00 MeV	60 000

6.00 MeV	70 000
7.00 MeV	90 000
8.00 MeV	100 000

3.4 MONTE CARLO OUTPUT

A sample of the pulse height spectra generated by the Monte Carlo code for the above neutron groups is presented in figure 3-1. A plot of neutron energy versus the light output bin corresponding to three quarters of the neutron peak height on the high energy side is presented in figure 3-2. This plot provides a general guide to the light output of the ONM as predicted by the Monte Carlo for incident monoenergetic neutrons.

Figure 3-3 is a plot of the Monte Carlo generated integral efficiency of the ONM for 2.45 Mev neutrons. In chapter 2 it was shown that the bias of the ONM is set at about 0.16 MeVee. From the Monte Carlo calculation this bias setting corresponds to an efficiency of about 32 percent. This efficiency is merely the efficiency of the plastic scintillator and does not consider important factors such as light transmission through the scintillator, the quality of the optical coupling between the scintillator and the photomultiplier tube, and the effects of the photomultiplier tubes and associated electronics.

Figure 3-1

Monte Carlo generated light output spectra for monoenergetic neutrons.

(a) Two MeV neutrons.

(b) Four MeV neutrons.

(c) Six MeV neutrons.

(d) Eight MeV neutrons.

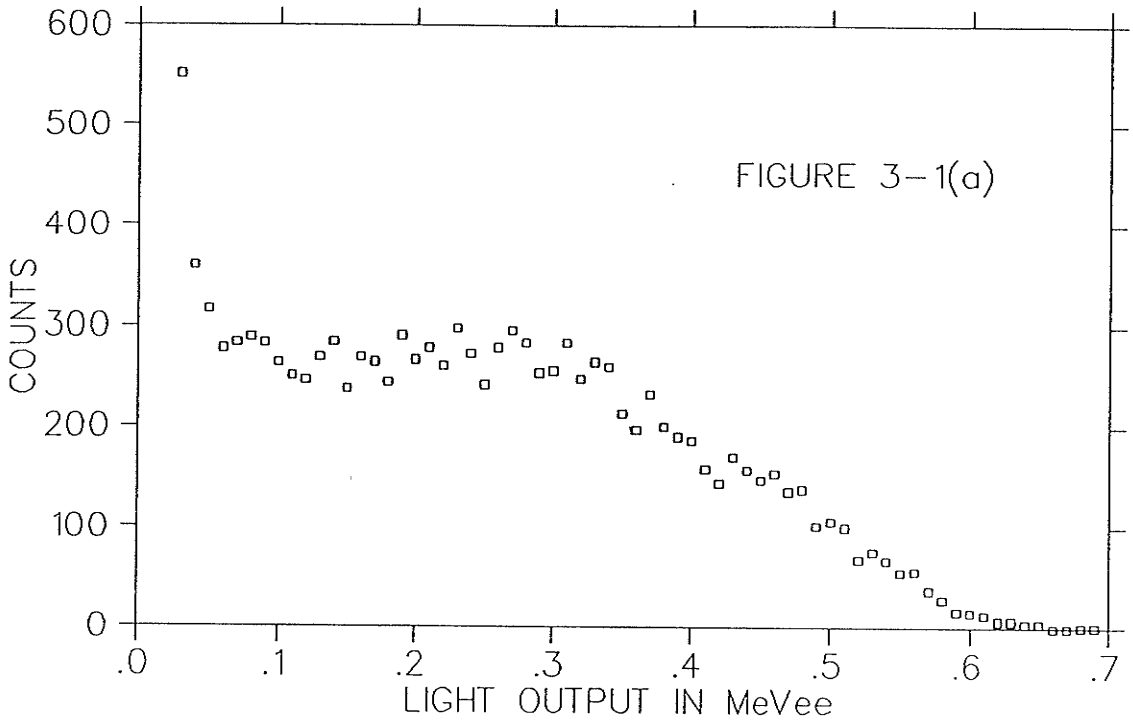

FIGURE 3-1(a)

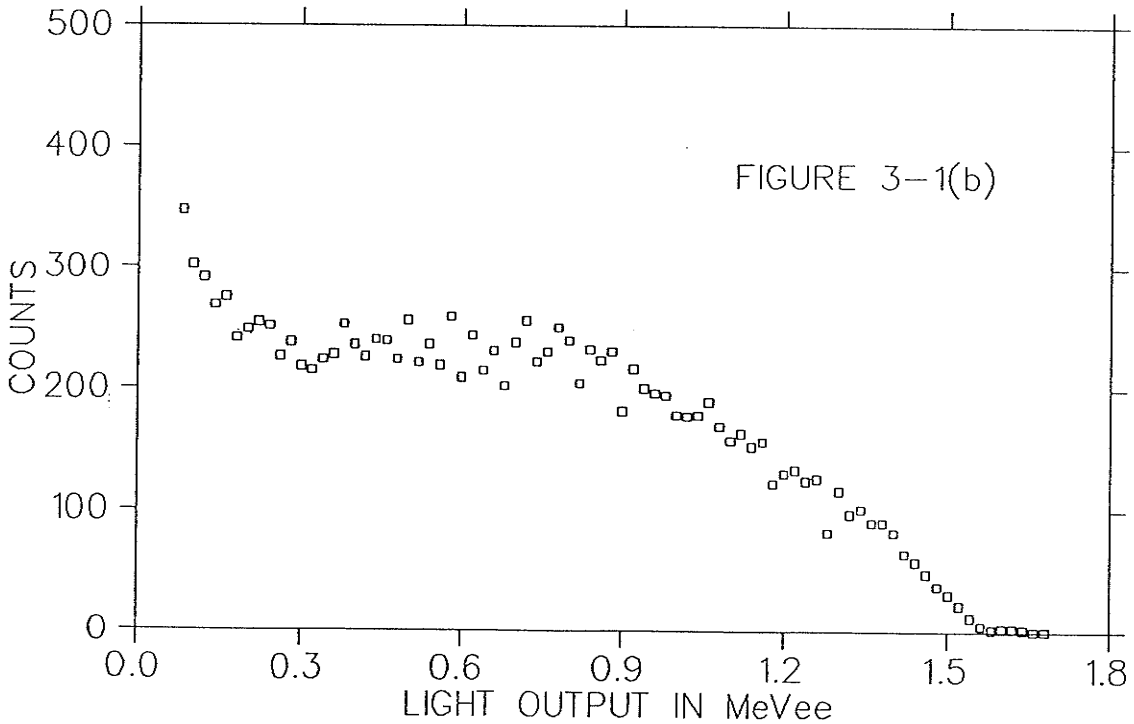

FIGURE 3-1(b)

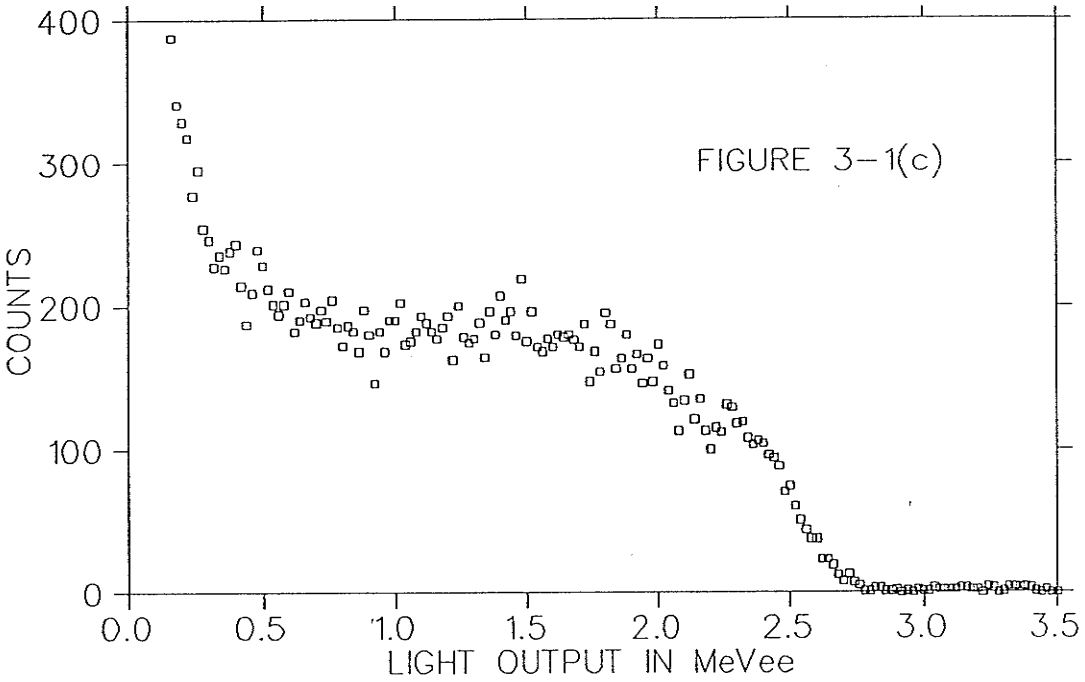

FIGURE 3-1(c)

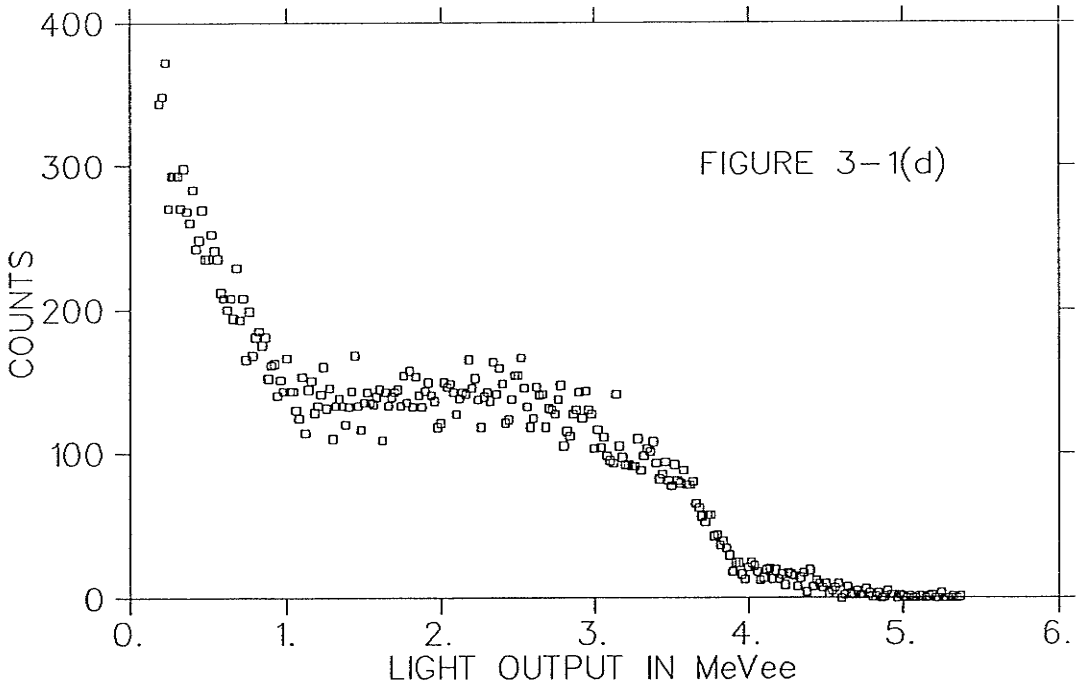

FIGURE 3-1(d)

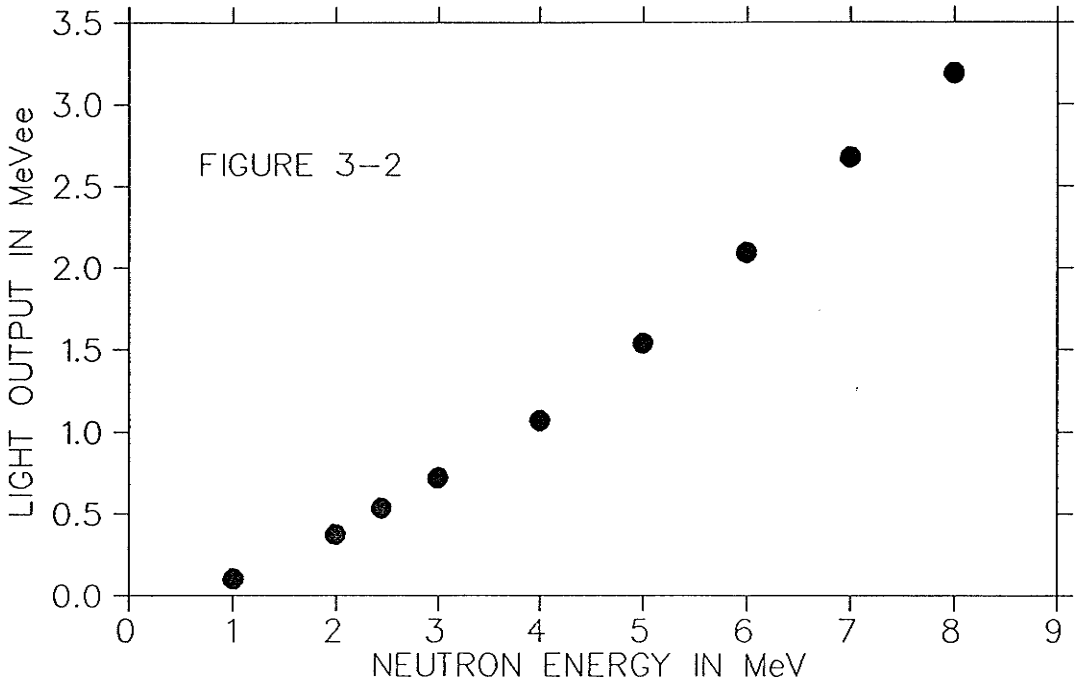

Figure 3-2

Light output corresponding to the three quarter position versus neutron energy.

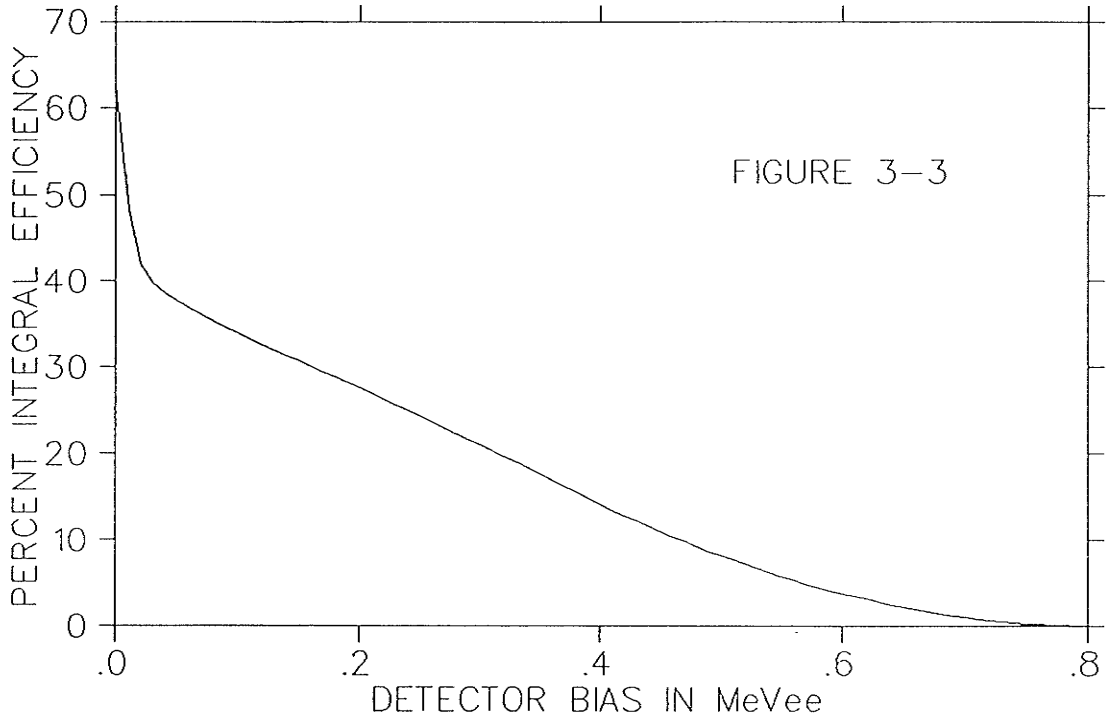

Figure 3-3

Monte Carlo generated integral efficiency of the ONM scintillator for 2.45 MeV neutrons.

CHAPTER FOUR

Exposure of the Online Neutron Monitor to Neutrons of Known Energy.

4.1 INTRODUCTION

The final step in the ONM calibration procedure is the exposure of the detector to a radioactive americium-beryllium (Am-Be) source of fast neutrons. Many of the neutrons emitted by the Am-Be source are accompanied by the simultaneous emission of a 4.44 MeV gamma ray. The time difference between the detection of the gamma ray in a suitable detector and the detection of the neutron in the ONM is measured. This information is used to calculate the time of flight of the neutron from the source to the ONM and ultimately the neutron energy (FI90). Using this technique, the energy of each neutron event in the ONM is known and ONM output spectra can be generated for different neutron energy groups and compared to the Monte Carlo predictions.

4.2 THE AMERICIUM-BERYLLIUM FAST NEUTRON SOURCE

In our neutron response study, the ONM was exposed to an alpha-Be fast neutron source. This source is a mixture of beryllium with one curie (3.7×10^{10} becquerel) of ^{241}Am. The americium is a source of alpha particles and the beryllium contains ^{9}Be. The alpha particle may combine with a ^{9}Be nucleus resulting in the creation of a ^{13}C nucleus in an excited state (see figure 4-1). The ^{13}C may decay to ^{12}C via the emission of a neutron. The decay to ^{12}C may proceed via several channels, one of which involves the first excited state of ^{12}C as an intermediate state. The first excited state of ^{12}C decays very quickly via an E2 transition resulting in the emission of a 4.44 MeV gamma ray (HA60).

The net interaction for the 4.44 MeV channel may be written:

$$^{9}Be + \alpha \text{ ---> } ^{12}C^{*} + n + 1.29 \text{ MeV}$$

$$^{12}C^{*} \text{ ---> } ^{12}C + \gamma \text{ (4.44 MeV)}$$

Therefore neutrons with energy equal to roughly the incident alpha energy plus 1.29 MeV will be produced via this process.

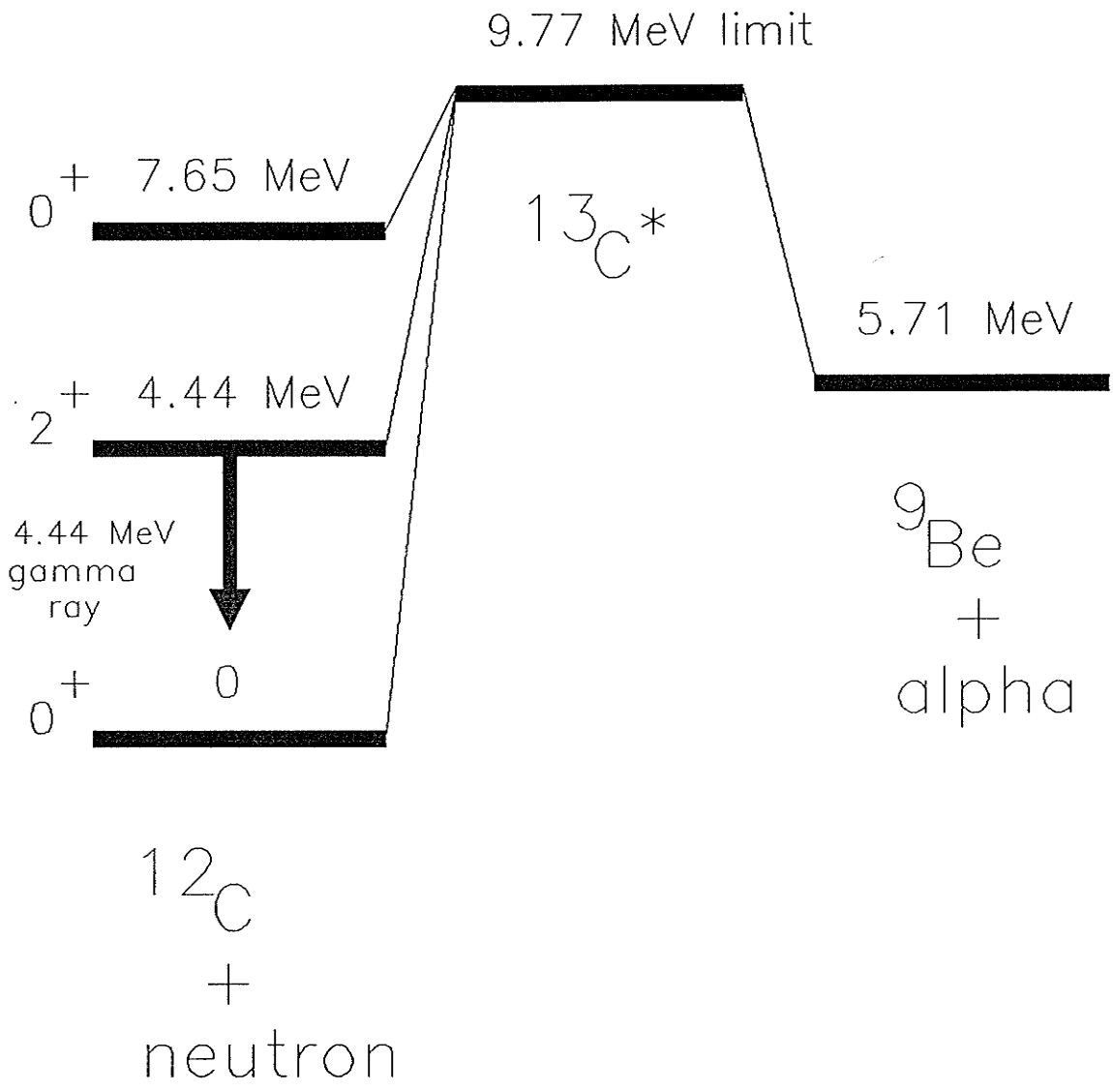

Figure 4-1

Neutron production process in an alpha-beryllium neutron source. 56% of the neutrons produced by the source are believed to be associated with the reaction:
$^{13}C^{*} \rightarrow {}^{12}C^{*} + n$
$^{12}C^{*} \rightarrow {}^{12}C + 4.44$ MeV (gamma).

^{241}Am decays via alpha emission virtually 100% of the time, with only three significant channels (BR86):

Alpha Particle Energy	Abundance
5.485 MeV	85.2%
5.443	12.8%
5.388	1.4%

The mean alpha particle energy is 5.480 MeV.

The half life of ^{241}Am is 432 years. The daughter substance is ^{237}Np which has a half life of 2 million years. If we assume that the americium was pure at point of manufacture 20 years ago it is reasonable to ignore the effects of ^{237}Np and any subsequent daughter substances.

It has been suggested that for an Am-Be neutron source, a neutron yield of about 70 neutrons per million alpha disintegrations is to be expected (RU56). The Manitoba source has a activity of about 4×10^{10} becquerel and thus a neutron yield of about 2.8×10^{6} is expected. Fifty six percent of these neutrons are believed to be associated with the emission of a 4.44 MeV gamma ray (KA86). Therefore, the neutron activity corresponding to the 4.44 MeV state for the Manitoba neutron source is estimated to be 1.6×10^{6} neutrons per second.

Kamboj and Shahani have measured the neutron flux corresponding to the 4.44 MeV state of a 500 millicurie Am-Be source to be 5.63 x 10^5 neutrons per second (KA86). This measurement would suggest that the flux of the Manitoba source is about 1.13 x 10^6 neutrons per second which is in general agreement with our estimate.

A detailed discussion of experimental and theoretical neutron spectra for an Am-Be neutron source is given by Vijaya and Kumar (VI73). In their theoretical calculation the authors have separately treated the ground, first excited and second excited states of ^{12}C. Vijaya and Kumar predict that the neutrons associated with the first excited state will range in energy between 1.7 and 6.4 MeV. The mean energy of these neutrons is about 4.2 MeV. However, a more recent paper by Coelho et al presents experimental data which suggests that the Vijaya spectrum is inaccurate in the lower energy region (CO89). Coelho, who measured the Am-Be neutron flux from 3 to 13 MeV using a NE-213 scintillator found that the neutron yield falls off abruptly at about 3.5 MeV and not 2.5 MeV as predicted by most theoretical calculations. A comparison of theoretical predictions and the results of Coelho are presented in a recent paper by Baldini et al (BA91).

It has been suggested by James et al that an angular correlation exists between the momentum of the gamma ray and the momentum of the neutron

(JA56). This correlation is maximum at 135 degrees. However, more recently other investigators have suggested that there is no significant correlation between the two radiations (BA91). In this work, a maximum correlation at 135 degrees was assumed.

4.3 THE TIME OF FLIGHT EXPERIMENTAL ARRANGEMENT

The experimental arrangement for the ONM calibration is shown in Figure 4-2. The large NaI crystal is used to detect the 4.44 MeV gamma ray. A pulse height spectrum of the neutron source obtained by the NaI detector is presented in figure 4-3. The presence of a peak at 4.44 MeV (full energy peak), a peak at 4.44 - 0.511 MeV (single escape peak) and a peak at 4.44 - 1.02 MeV (double escape peak) suggests a pair production interaction involving a 4.44 MeV gamma ray. This strongly suggests the existence of the first excited state of ^{12}C in the neutron source.

The large peak at 2.2 MeV in the pulse height spectrum is likely due to the gamma ray emitted in the radiative neutron capture reaction occurring in the H_2O neutron shielding which surrounds the source (SE77):

$$n + p \rightarrow d + \gamma\ 2.22\ MeV$$

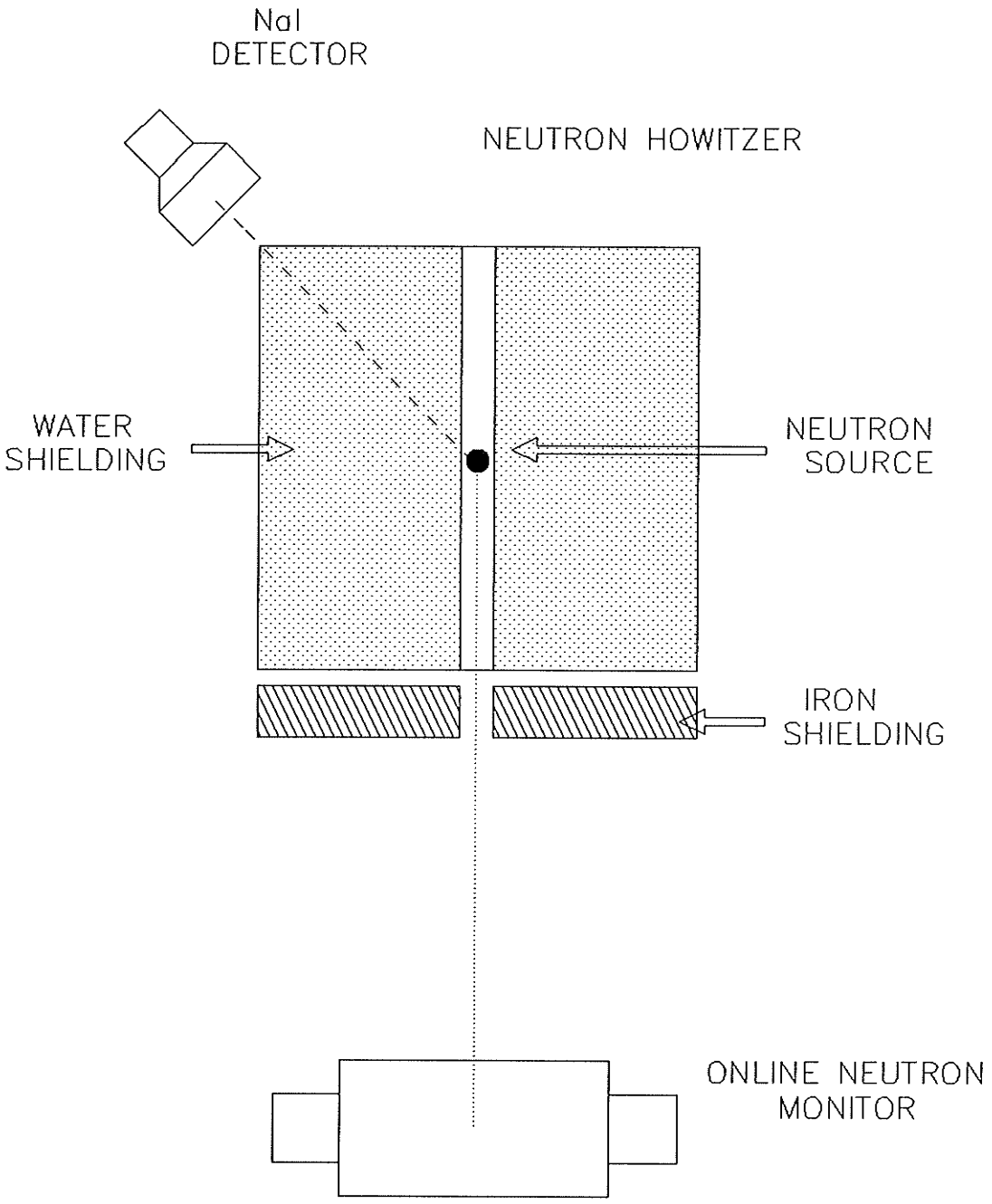

FIGURE 4–2

Neutron time of flight
experimental arrangement.

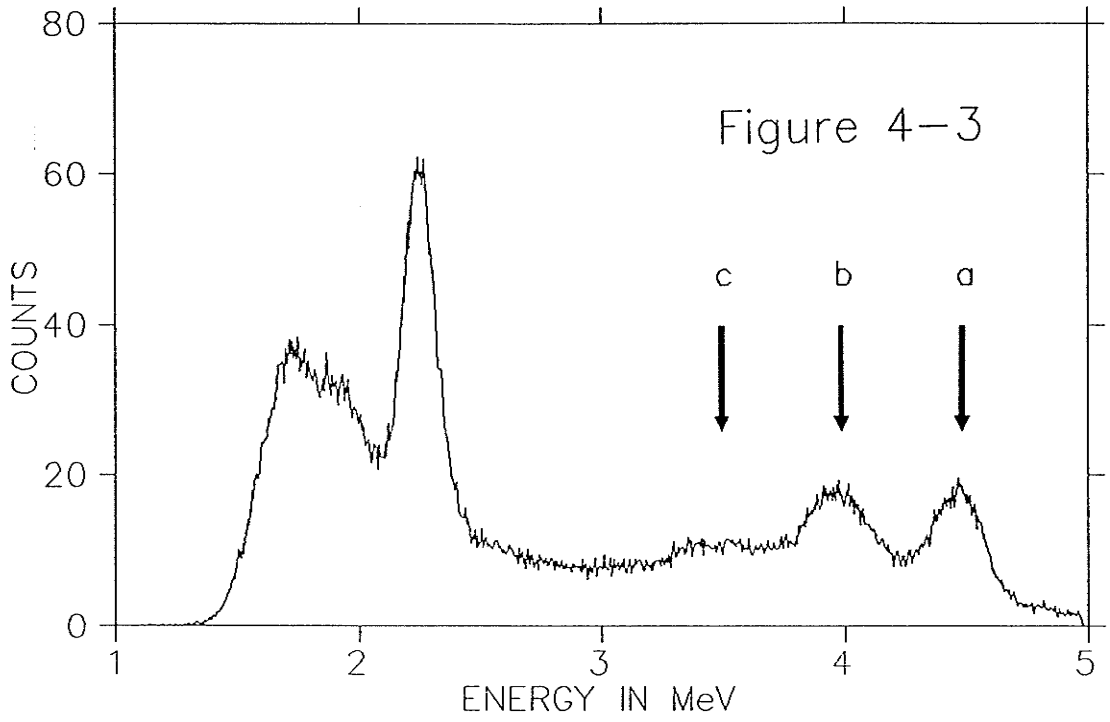

Figure 4-3

Gamma ray spectrum of the Am-Be neutron source showing structure due to 4.44 MeV and 2.2 MeV gamma rays.

a - Full energy peak for 4.44 MeV gamma ray.

b - Single escape peak associated with 4.44 MeV gamma ray.

c - Double escape peak associated with 4.44 MeV gamma ray

The ONM is positioned a distance D from the source. In this work a D of 2 metres is used. The energy of a neutron En, is related to T, the time difference between the signals from the ONM and the NaI detector, by the following relation:

$$E_n = (72.3\ D\ /\ (T + 1.6\ ns))^2 \qquad \text{Equation 4-1}$$

Where E_n,D and T are expressed in units of MeV, metres and nanoseconds respectively. The extra 1.6 ns is added to compensate for the time of flight of the gamma ray from the source to the NaI detector (1.3 ns) and the separation of the NaI detector and ONM during the cosmic ray time calibration (0.3 ns) The uncertainty in E_n is related to the uncertainty in T by the following relation:

$$\Delta E_n = E_n\ [(2\Delta T/T)^2 + (2\Delta D/D)^2] \qquad \text{Equation 4-2}$$

The uncertainty in time ΔT is due to the finite time resolution of the system. The uncertainty in the flight path ΔD is due to the finite thickness of the ONM and the finite thickness of the neutron source.

The neutron source is placed in a 'Neutron Howitzer' which provides a beam of fast neutrons. The howitzer (see figure 4-2) is a rectangular tank of water. The neutron source sits in the centre of the tank. A tube which leads from the centre of the tank to the tank wall provides a moderator free 'beam line' path for fast neutrons. The NaI crystal is located 43.1 cm from the source at an angle of 135

degrees to the howitzer beam line.

4.4 THE TIME OF FLIGHT DATA ACQUISITION SYSTEM

A block diagram of the electronics used in the Time Of Flight (TOF) data acquisition system is shown in figure 4-4. The electronics associated with the ONM is identical to the configuration used in the COLLECT system (Figure 1-2). In the TOF system a start pulse is generated when an event is detected in the ONM. The time to digital converter (TDC) counts until a stop pulse has been received from the NaI detector, or until the TDC overflows. Although the gamma ray reaches the NaI crystal about 80 ns before the neutron reaches the ONM, the relatively slow response time of the NaI timing system compared to the ONM timing system means that a timing pulse is generated by the ONM before a timing pulse is generated by the NaI detector.

It is also advantageous to start the TDC with a pulse from the ONM because the counting rate in the ONM is less than the counting rate in the NaI detector. Because the TDC will count until it overflows, the dead time of the system is proportional to the start rate.

The zero or prompt of the system must be determined before any time of flight measurements can be made. The prompt is the position in the time spectrum

FIGURE 4–4

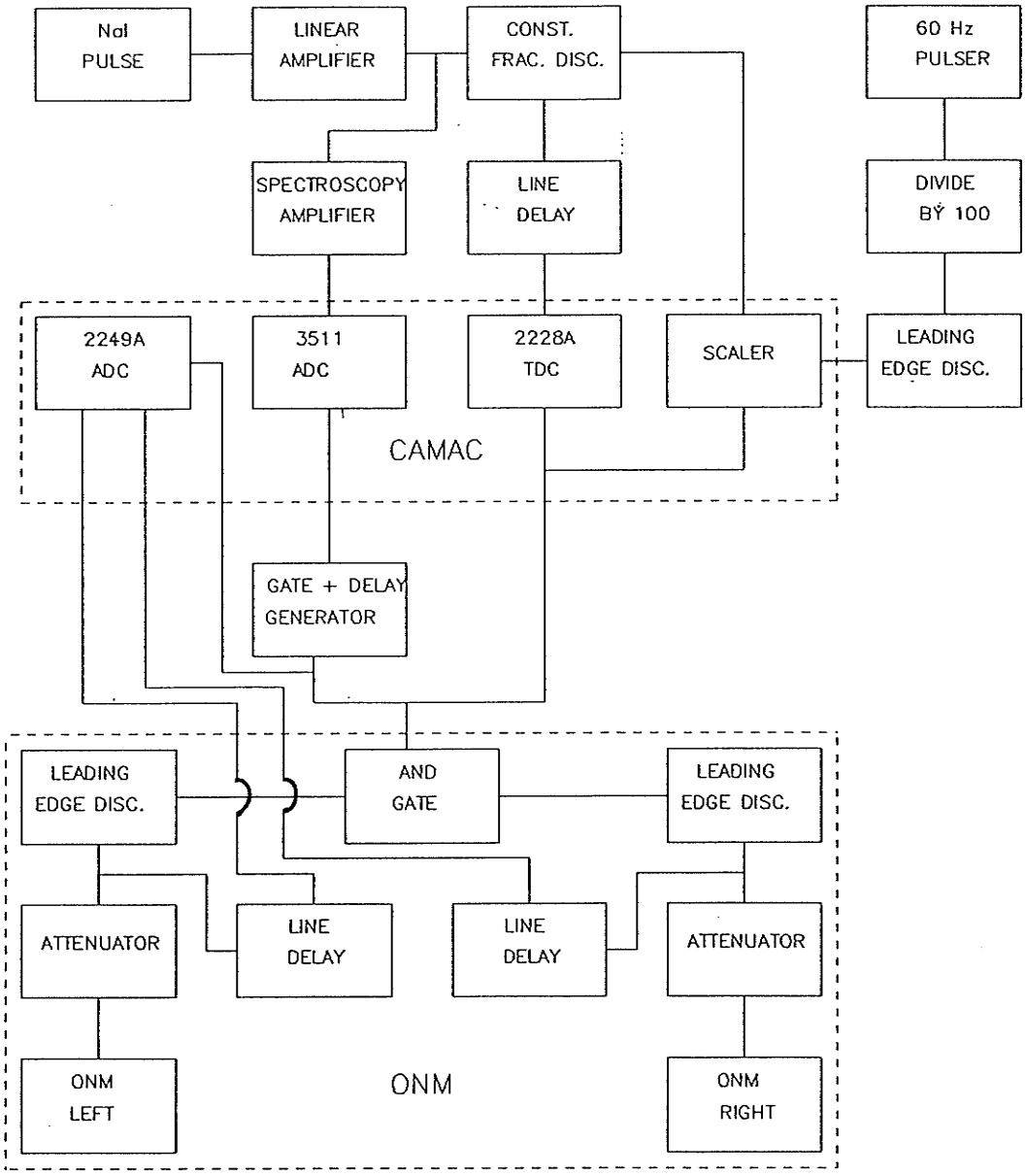

Time of flight electronics.

which corresponds to an event which occurs simultaneously in both detectors. To determine the prompt position the NaI detector is placed on top of the ONM, with a separation of 5 cm. Cosmic rays may traverse both detectors and are easily detected. The cosmic rays are highly relativistic and thus a separation of 5 cm corresponds to a time delay of 0.33 ns. A time spectrum of these cosmic muons is presented in figure 4-5. The intrinsic delay of the system is about 125.5 ns, the prompt peak in figure 4-5 is shifted another 63.5 ns by delaying the signal from the NaI detector. As a result the prompt peak is at 189 ns with a standard deviation of 3.5 ns.

Cosmic muons deposit significantly more energy in the NaI crystal then do 4.44 MeV gamma rays. In the normal operating mode, the pulse from a muon is severely clipped by the Phillips preamplifier and thus has a very different shape than a pulse corresponding to a 4.44 MeV gamma ray. The timing pulse for the NaI system is produced by a constant fraction discriminator, which is very sensitive to pulse shape. Therefore, the TOF system must be modified slightly in order to perform the time calibration with the cosmic muons. The PMT signal from the NaI detector is attenuated using a resistive network such that the pulse shape for a muon event is similar to that of a 4.44 MeV gamma ray in the normal operating mode. The attenuation factor used is ten percent. In the ONM system the signal from a cosmic ray event is also much larger than that associated with a neutron event. To correct for this each signal from the two ONM photomultiplier tubes was

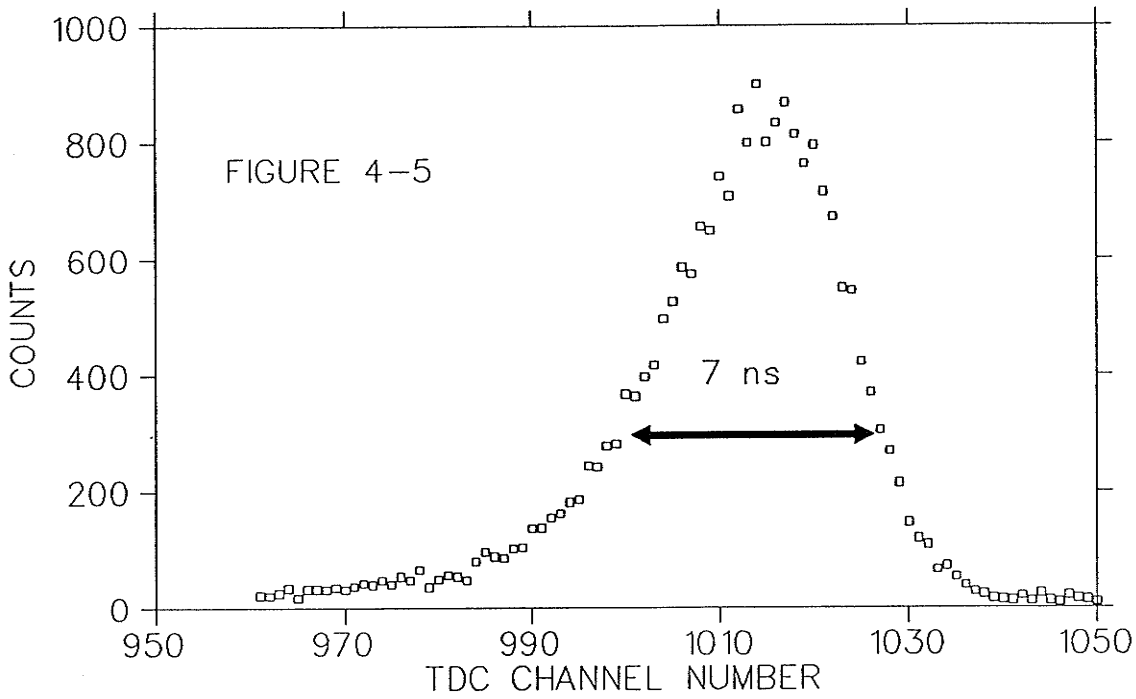

Figure 4-5

The time of flight spectrum (detail) of cosmic muons which traverse both the NaI detector and the ONM during the prompt calibration.

attenuated to 20% of the original pulse size.

4.5 THE DATA ACQUISITION PROCESS

The operation of the TOF system is fully automated through the use of a CAMAC crate and a microcomputer. A discussion of the CAMAC hardware and software and a full listing of the TOF data acquisition code is provided in the appendix to this thesis.

A timing signal from the ONM AND gate starts the time to digital converter (TDC) and provides a gate pulse to the 2249A ADC which digitizes both channels of the ONM. The signal from the AND gate also generates a gate signal for the 3511 ADC. Thus, whenever an event is detected in the ONM the signal from the NaI is digitized regardless of whether it corresponds to a valid event or not.

When the TDC has stopped counting it will generate a look at me (LAM), telling the CAMAC system and the computer that an event has been digitized. The computer retrieves the time information from the TDC and determines if the TDC has overflowed, which corresponds to a start pulse which was not followed by a stop pulse in an appropriate time interval. If an overflow is detected, both ADC's and the TDC are cleared and the system waits for another event. If no overflow has occurred, the data from both ADC's is retrieved and stored on the computer

hard disk along with the time information. Each valid event contains four pieces of information: The time of flight, the NaI detector pulse height, and the pulse size of both ONM channels. For online diagnostics, the data is histogrammed as it is collected and the operator may interrupt the data acquisition process at any time to view the histograms.

The total number of events in the ONM and the NaI detector are monitored by the CAMAC scaler. The run time of the experiment is also monitored by the CAMAC scaler through the use of a 60 Hz pulser and a divide by 100 counter. At the end of a run the scaler is read, and this information, along with histograms of the ONM, TDC and NaI detector are stored on the computer hard disk.

4.6 RESULTS AND ANALYSIS

4.6.1 THE TIME OF FLIGHT SPECTRUM

The first step in the analysis procedure is the creation of a time of flight histogram from the timing data. The time data is processed in the following manner:

1) Each time to digital converter datum is subtracted from the prompt channel to yield a difference of channel numbers.

2) The difference of channel numbers is converted to a time difference in nanoseconds using an appropriate calibration factor.

3) The data is histogrammed as counts versus time difference or time of flight.

Such a histogram is presented in figure 4-6. The structure centred at 0 ns is believed to be the result of cosmic ray showers of very short duration which cause near coincident events in both detectors. The structure between 45 and 100 ns is believed to be the time of flight spectrum of the neutrons associated with the 4.44 MeV gamma ray.

In figure 4-6 it is evident that both the cosmic ray and neutron structures are riding on top of a rather significant background level. This background is believed to be the result of random coincidences which are known to make up a significant percentage of all events detected.

The background rate from random coincidences may be measured directly by adding a further delay of about 110 microseconds to the stop pulse. Then the time of flight experiment is run in the usual manner. A delay of 110 microseconds is three orders of magnitude longer than the time associated with real events and thus it may be assumed that all events detected in this configuration are indeed random coincidences. In this mode of operation the random event rate is

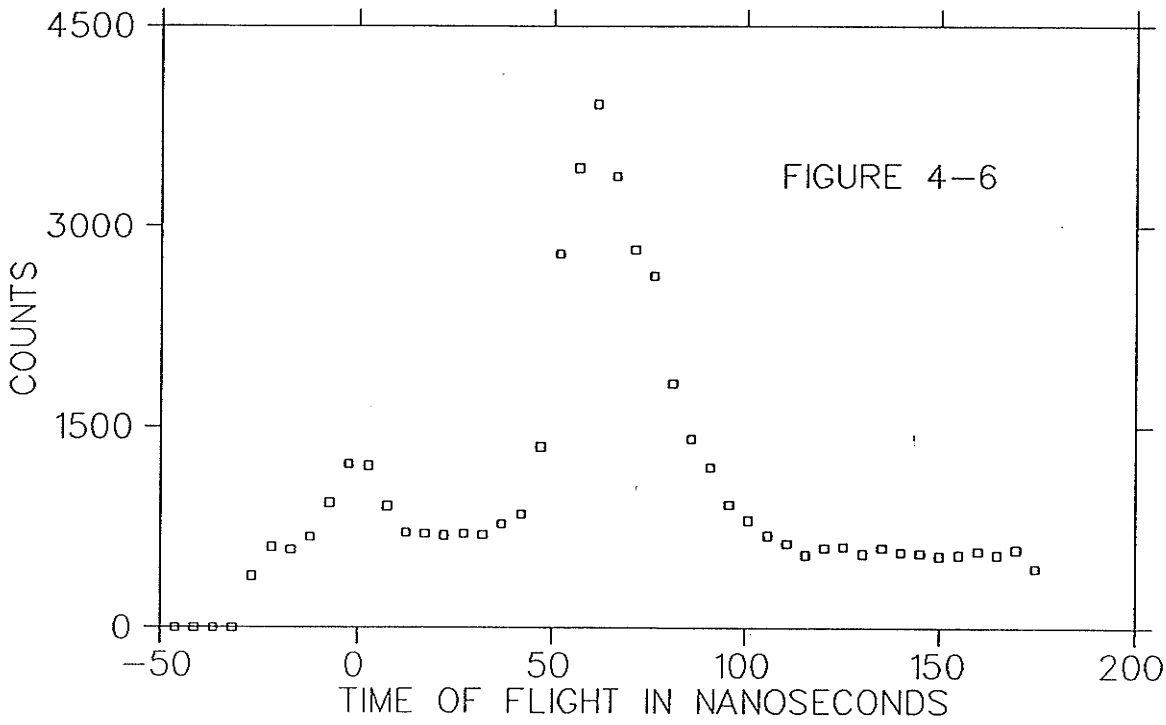

Figure 4-6

Time of flight spectrum of events detected with the TOF system.

measured as 0.0751 Hz. In the normal time of flight mode, the event rate is 0.1130 Hz. Therefore random coincidences account for about 66% of all events registered in the normal time of flight configuration.

4.6.2 THE NEUTRON ENERGY SPECTRUM

The next step in the data analysis procedure is the generation of a neutron energy spectrum from the time of flight data via equation 4-1. Because of the nonlinear nature of the energy-time relationship, great care must be taken creating an energy histogram in which the background due to random events is properly subtracted. The following procedure was devised to create a background subtracted neutron energy distribution from the time of flight data:

1) An energy value is generated for each time of flight event using equation 4-1 and the energy data is histogrammed.

2) A flat, background-like set of time of flight data points is generated to synthesize the random coincidence spectrum obtained by delaying the stop pulse by 110 microseconds. This background-like set is then normalized to represent the background present in the time of flight data.

3) A background energy histogram is generated from the data set created in step 2. This background histogram is then subtracted from the histogram generated in step 1, providing a background subtracted energy spectrum of the neutrons detected with the time of flight apparatus.

The background subtracted neutron energy spectrum is presented in figure 4-7. This energy spectrum is in reasonable agreement with the theoretical predictions of the neutron spectrum associated with the 4.44 MeV gamma ray made by Vijaya and Kumar (VI73). In the energy region between about 1.5 and 6.0 MeV the agreement is quite good but at energies greater than about 6.0 MeV there is disagreement with the current theoretical predictions which indicate that the upper limit of the energy spectrum should be at about 6.4 MeV. As well, if the energy level diagram presented in figure 4-1 is accurate it is clear that neutron energies greater than about 6.5 MeV are energetically forbidden. At the present time the presence of these energetically forbidden neutrons in the time of flight spectrum is not well understood and might ultimately reflect an error in the theoretical calculation or a yet undetermined experimental oversight.

The appearance of energetically forbidden neutrons in the neutron energy spectrum may be the result of a systematic error in the measurement of the neutron time of flight. There are two important factors involved in this measurement, the time calibration of the time to digital converter and the

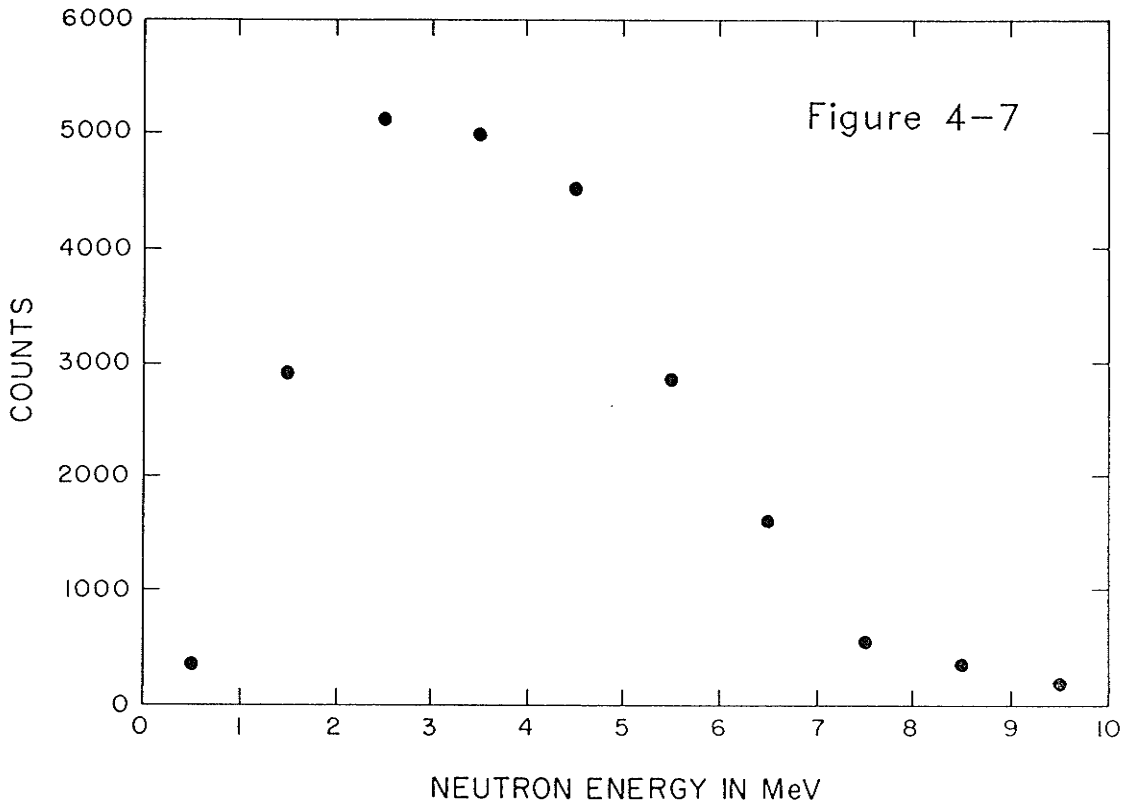

Figure 4-7

Neutron energy spectrum from neutron time of flight data. Background subtraction has been performed. The histogram has a bin width of one MeV. The uncertainty in the neutron energy is a function of neutron energy (see equation 4-2) and is less than one MeV for neutron energies less than eight MeV.

determination of the prompt position in the time spectrum (see section 4.4). After the data presented in this chapter was obtained, the time to digital converter was recalibrated using the output from a pulse generator, delay lines and an oscilloscope. It was found that the time calibration had not changed during the course of the time of flight measurement.

In addition, the prompt position in the time spectrum was determined before and after the time of flight measurement and was found not to have changed significantly. However, it is possible that the method used to obtain the prompt position has a systematic error associated with it. If the time of flight measurement is to be repeated, it is recommended that additional methods are devised to determine the prompt position and the results compared for consistency.

An obvious alternate method of measuring the prompt position would employ a Compton scattering experiment similar to that described in chapter 2. The time difference between the detection of the Compton electron the ONM and the detection of the scattered gamma ray in the NaI crystal would provide the prompt position.

4.6.3 THE ONM SPECTRA

Using the neutron energy spectrum of figure 4-7 as a guide, the neutron events were divided into three energy groups. The following groups were defined.

Low Energy	1.5 to 3.2 MeV	(9 046 events)
Medium Energy	3.2 to 4.8 MeV	(10 867 events)
High Energy	4.8 to 6.5 MeV	(7 917 events)

An ONM pulse height spectrum for each of the above energy groups was generated from the data. These spectra are presented in figure 4-8(a). Because a large percentage of the events included in these spectra are due to random coincidences it is prudent to subtract the ONM spectrum associated with random coincidences from gross spectra of figure 4-8(a). The following background subtraction scheme was employed:

1) Events corresponding to a time of flight between 175 and 225 ns were identified as background coincident events by comparing the ONM spectrum of this group with the ONM spectrum obtained from the random coincidence data.

2) An ONM spectrum was generated from these events.

Figure 4-8(a)

ONM spectra for the three neutron energy groups:

□ Low energy group (1.5 to 3.2 MeV)

+ Medium energy group (3.2 to 4.8 MeV)

◇ High energy group (4.8 to 6.5 MeV)

Figure 4-8(b)

ONM spectrum for random coincidence events.

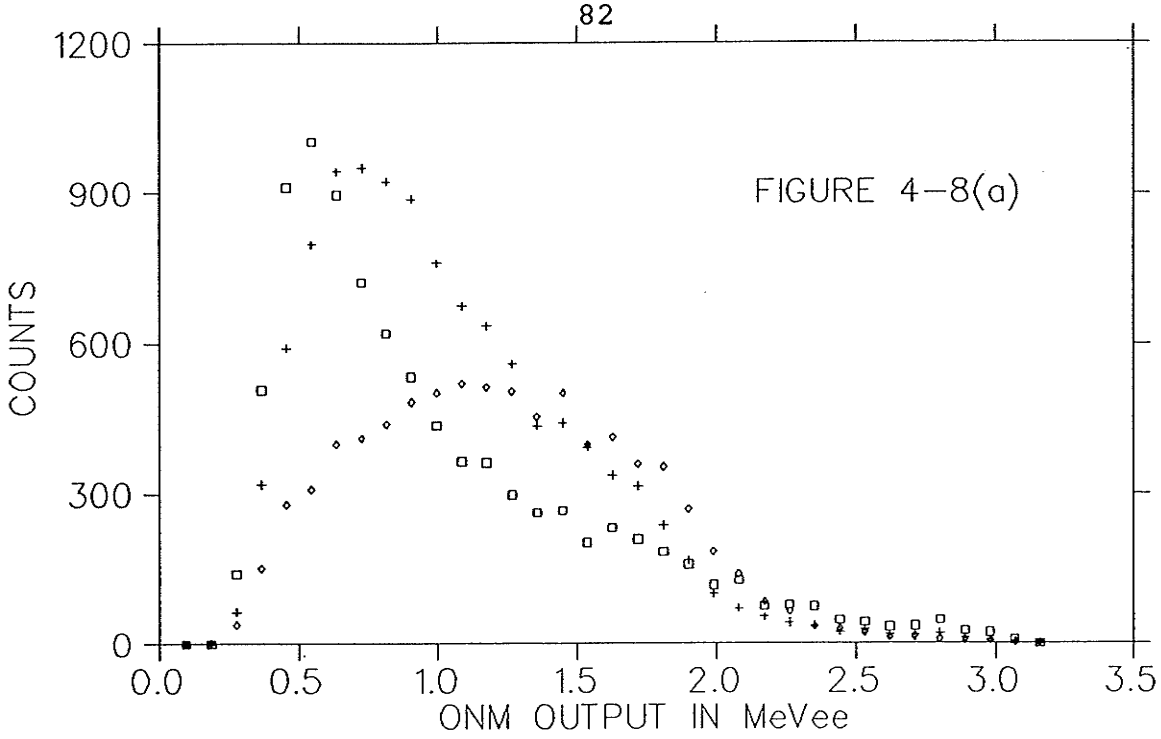

FIGURE 4-8(a)

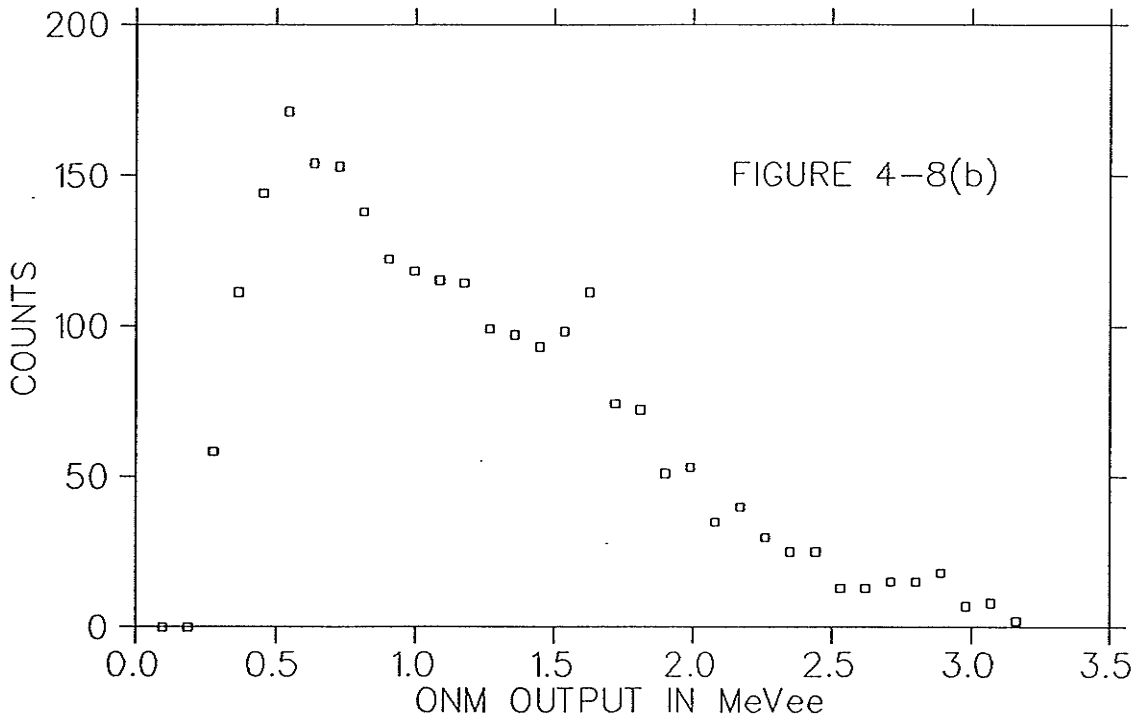

FIGURE 4-8(b)

3) A normalized background spectrum for each of the low, medium and high neutron groups was generated from the spectrum of step 2 according to the number of time channels in each group.

4) A background subtraction for each neutron group was performed.

The background spectrum associated with the random coincidences is shown in figure 4-8(b). Figure 4-8(c) shows the background subtracted low, medium and high energy ONM spectra. As expected, the ONM spectra tend to shift to the right or greater light output region with increasing neutron energy.

4.6.4 COMPARISON WITH MONTE CARLO PREDICTIONS

The final step in the analysis of the ONM response is a comparison of the low, medium and high energy neutron groups with Monte Carlo generated spectra. Such a comparison is a test of the applicability of the Monte Carlo code to the ONM.

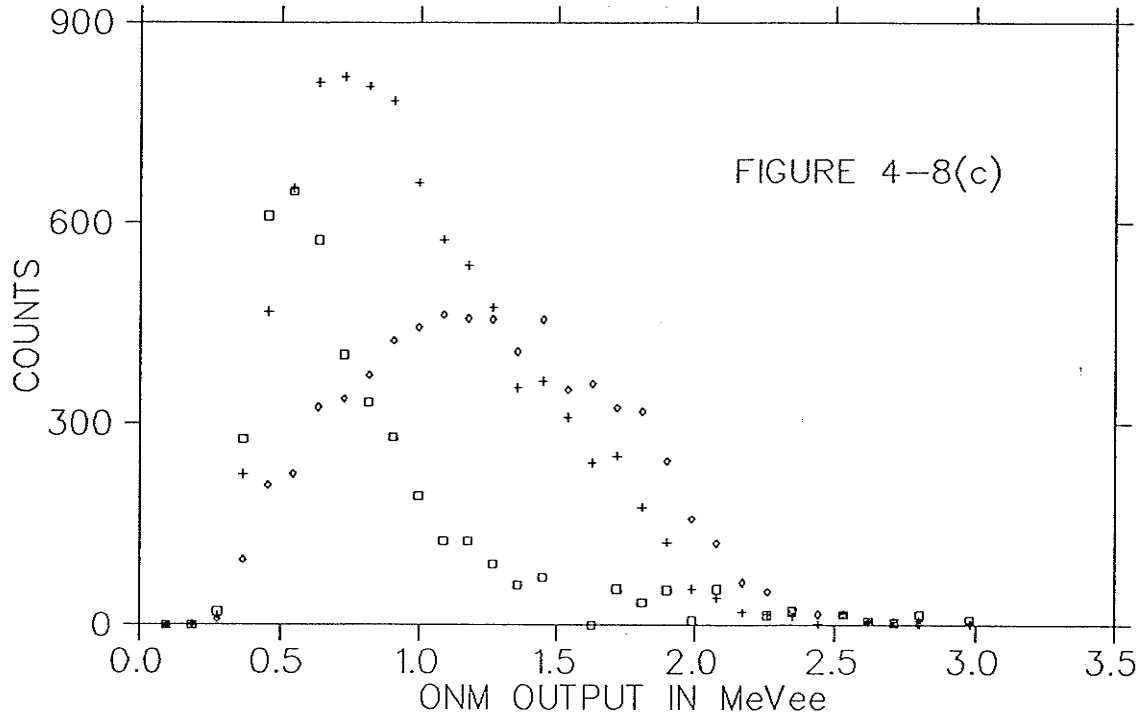

Figure 4-8(c)

Background corrected ONM spectra for the three neutron energy groups:

- □ Low energy group (1.5 to 3.2 MeV)
- \+ Medium energy group (3.2 to 4.8 MeV)
- ◊ High energy group (4.8 to 6.5 MeV)

The Low Energy Neutron Group

In the energy region between 1.5 and 3.2 MeV the neutron energy distribution changes rapidly (see figure 4-7). In an attempt to define a neutron group in this energy region for the Monte Carlo code the following groups of monoenergetic neutrons were used to generate a Monte Carlo light output spectrum.

Neutron Energy	Number of Neutrons
1.6 MeV	7 000
2.0	15 500
2.4	24 740
2.8	34 000
3.2	44 000

Figure 4-9(a) presents both the low energy group ONM spectrum and the Monte Carlo generated spectrum for comparison.

The Medium Energy Neutron Group

In the energy region between 3.2 and 4.8 MeV the neutron distribution is reasonably flat and a Monte Carlo simulation was generated which employs a random distribution of neutrons with energies between 3.2 and 4.8 MeV. Figure 4-9(b) shows both the medium energy ONM spectrum and the Monte Carlo

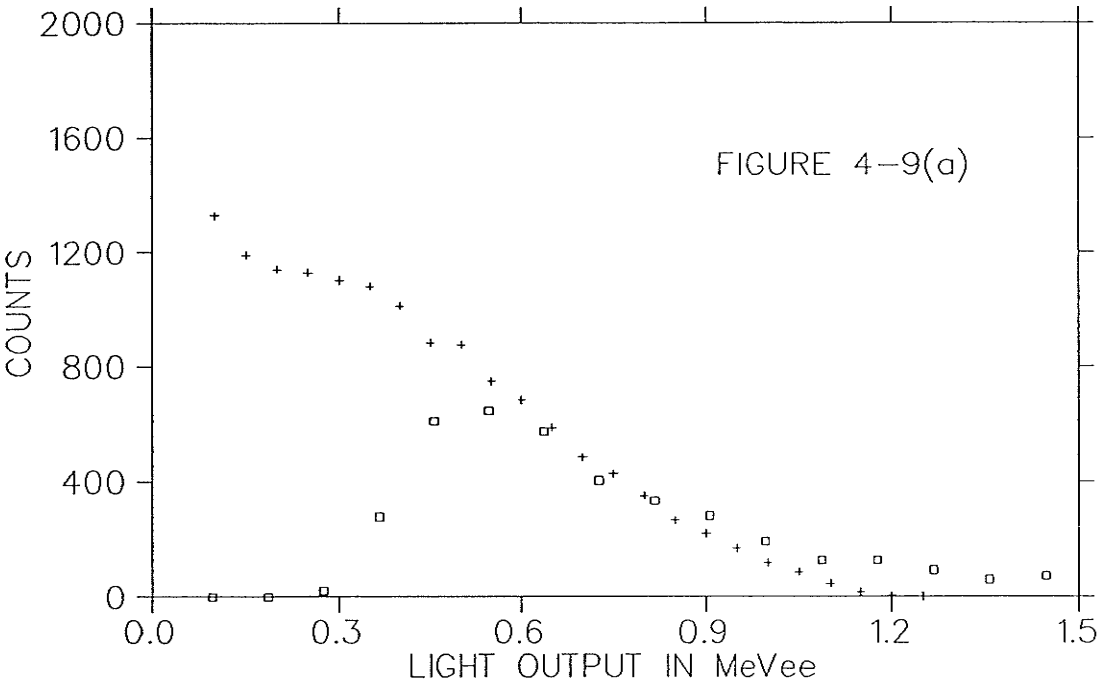

Figure 4-9(a)

Comparison of the Monte Carlo generated light output spectrum (+) and the ONM spectrum (□) for the low energy neutron group.

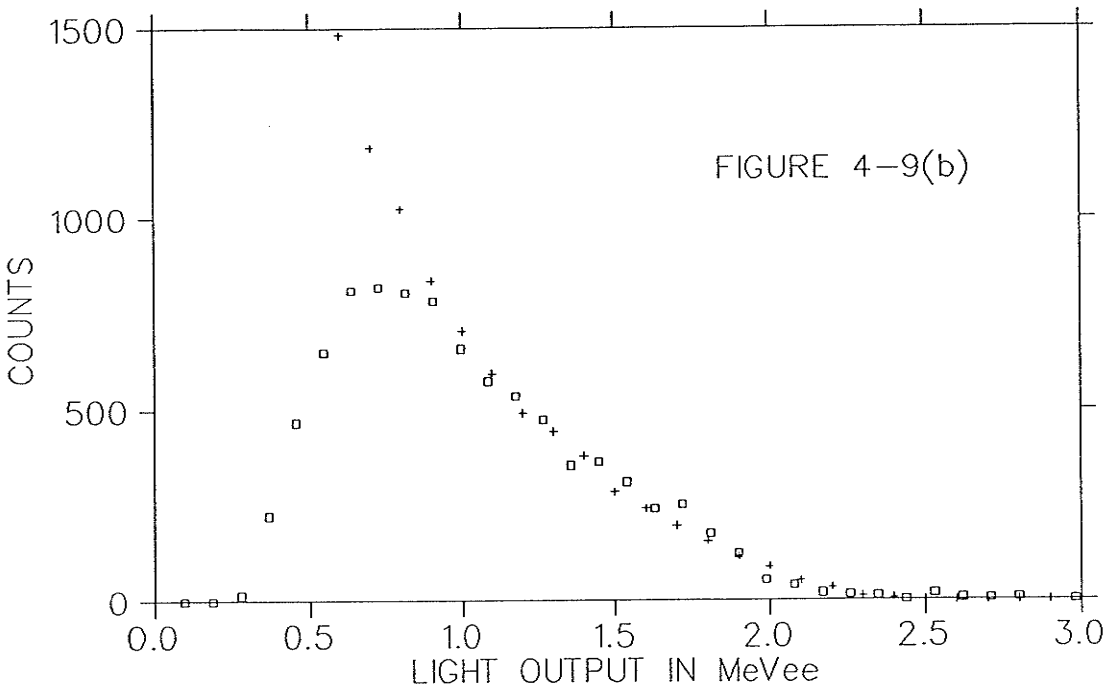

Figure 4-9(b)

Comparison of the Monte Carlo generated light output spectrum (+) and the ONM spectrum (□) for the medium energy neutron group.

generated spectrum for comparison.

The High Energy Neutron Group

In the region between 4.8 and 6.5 MeV the neutron energy distribution changes rapidly and therefore a five point distribution of monoenergetic neutrons was employed. A Monte Carlo simulation of the high energy group was performed with the following input.

Neutron Energy	Number of Neutrons
4.8 MeV	42 000
5.2	50 000
5.6	32 000
6.0	28 000
6.4	24 000

The high energy spectrum and the Monte Carlo prediction are presented in figure 4-9(c) for comparison.

4.7 DISCUSSION

In general, the agreement between the ONM experimental spectra and the Monte Carlo predictions is quite encouraging and suggests that the Monte Carlo

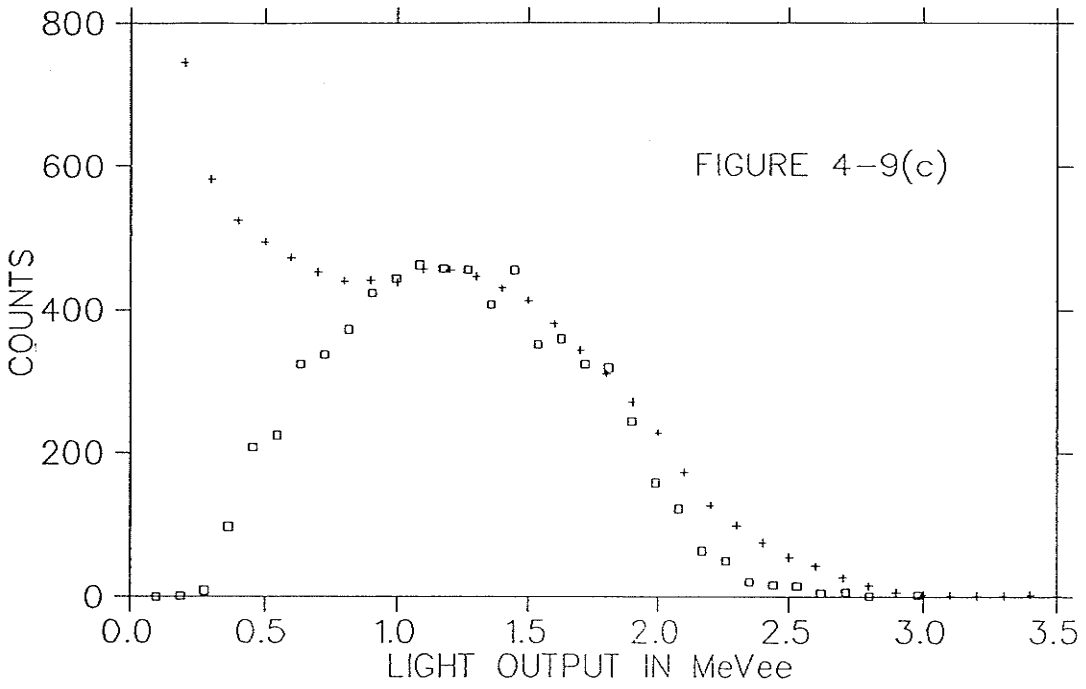

Figure 4-9(c)

Comparison of the Monte Carlo generated light output spectrum (+) and the ONM spectrum (□) for the high energy neutron group.

analysis has a usefulness in predicting the behaviour of the ONM. Agreement appears to be the best with the medium energy group and poorest with the low energy group. However, in all three groups there appears to be a consistent disagreement in the low energy portion of the spectrum.

In the low energy part of all three spectra, the Monte Carlo prediction appears to be systematically much greater than the experimental measurements. It is believed that this effect is caused by the lower level discrimination process that occurs in the ONM.

In the ONM, the signal from each of the photomultiplier tubes is fed into a separate lower level leading edge discriminator. If both discriminators fire within a set time interval, a gate pulse is supplied to an analog to digital converter which separately digitizes each photomultiplier pulse. Because the photomultiplier tube noise is rather high the two leading edge discriminators must be set relatively high to ensure that random coincidences due to noise do not dominate the system.

If a light producing event in the scintillator occurs closer to one photomultiplier tube than the other the signal from the far tube may be significantly less than the signal from the near tube for two reasons.

1) The light is attenuated as it travels through the scintillating material, the

intensity decreasing exponentially with distance.

2) The farther away the light source is from the photomultiplier tube, the smaller the solid angle for the direct transmission of light to the photomultiplier tube photocathode and an increase in the amount of light which reaches the photocathode via multiple internal refections. The direct path is much shorter than the reflected path and thus this light is not attenuated as much. This problem is very significant in the ONM because the photomultiplier tubes are separated from scintillating material by only a very thin lucite light guide which serves to couple the flat faces of the scintillator to the curved windows of the photomultiplier tubes. Direct transmission must account for a substantial portion of the light which is collected from events occurring close to the ends of the scintillator.

If a light producing event occurs closer to one tube than the other it is quite possible that the amount of light that reaches the far tube is insufficient to fire the discriminator even though, if the event occurred in the middle of the detector the amount of light reaching both detectors would be sufficient to fire both discriminators. This behaviour would lead to a decrease in the efficiency of the detector. This reduction in efficiency would be greatest in the lower region of the light output spectrum where the possibility that the far tube will not fire the discriminator is greater. The Monte Carlo code does not incorporate this lower level discrimination process and this may explain why the Monte Carlo consistently

predicts a greater event rate in the lower region of the light output spectrum for all three neutron groups.

During the data acquisition process, the analog to digital converter which digitizes the signals from the ONM acts as an effective upper level discriminator. The maximum photomultiplier tube pulse that may be digitized corresponds to a light output of 2.92 MeVee. As in the case of the lower level discrimination, the effective upper level discrimination is dependent upon the position of the light producing event.

If the light producing event occurs close enough to a tube to cause an overflow in the analog to digital converter the event will have to be discarded. Therefore events which would have been successfully recorded if they had occurred at the centre of the scintillator may be discarded when they occur closer to one tube. This effect would tend to lower the efficiency of the detector, particularly in the high end of the light output spectrum and thus primarily effect the detector response to higher energy neutrons.

In figure 4-9(c), it is apparent the ONM high energy neutron group light output spectrum and the Monte Carlo generated spectrum agree in the midrange region but disagree both in the high and low light output region. It is possible that the disagreement in the high light output end of the spectrum may be caused by the

upper level discrimination effect of the analog to digital converter.

Upon comparison of the medium energy group (figure 4-9(b)) and the high energy group it is apparent that the Monte Carlo is much better at predicting the upper portion of the medium energy spectrum than that of the high energy spectrum. The Monte Carlo simply creates a light output spectrum from the total light output of the simulated event and does not include the upper and lower level discriminations processes particular to ONM. In the medium neutron energy group it is possible that the light output is sufficiently low for all events such that the overflow upper level discrimination process is not significant.

Another area of concern in the operation of the ONM is the effect of background radiation. In the present set up the ONM detects background radiation with a coincidence rate between both tubes of about 297 Hz. It is believed that most of this background is due to environmental gamma rays. Some of the background, about 5 to 10 percent may be the result of cosmic muons. The COLLECT data acquisition system in the present state is able to digitize these background events at a rate of 181 Hz. Thus, 40 percent of all events are lost due to dead time caused by the large background rate.

This background will generate data at a rate of 2200 bytes per second or about 7.9 megablocks per hour of VAX storage space. If a week-long program of

experimental runs is undertaken, a staggering 1.32 gigablocks of storage space will be needed for the ONM background alone. The management of such a large amount of data would require the use of a tape storage device as such an amount of data would quickly fill the disk storage capabilities of the physics department.

4.8 RECOMMENDATIONS FOR IMPROVEMENT OF THE ONM

Although it has been demonstrated that the ONM is capable of detecting 2.45 MeV neutrons, it is clear that there are several severe restrictions on the use of the ONM in a low neutron event study. What follows is a set of recommendations that may be implemented to improve the performance of the ONM as a detector of fast neutrons for the Narodny ion implantation experiment.

1) If possible, the NE-102 scintillator should be replaced with a material such as NE-213 which would provide the opportunity to perform pulse shape discrimination. Pulse shape discrimination would greatly reduce the number of events stored as valid data by providing a method to discriminate between gamma ray events and neutron events.

2) The scintillating volume should be reduced. This would reduce the background counting rate by reducing the efficiency of the detector for background radiation. At the present the scintillator is a right cylinder with a diameter of 13.5 cm and

height of 33.5 cm. The target chamber in which the ion implantation occurs is a 13 cm cube. It is suggested that the ONM height be reduced to 15 cm so that it just covers the face of the beam cube. Such a geometry, if placed next to the beam cube would still be able to cover a significant portion of the neutron solid angle and the reduction in volume should result in a reduction in the background rate. A reduction in the height of the scintillating volume may also reduce the problem of position sensitive discrimination by reducing the distance between the photomultiplier tubes.

3) The light collection design of the ONM should be modified such that the possibility of direct light transmission from the scintillator to the photomultiplier tube photocathode be significantly reduced. This might be accomplished by utilizing long, converging lucite light guides and smaller photomultiplier tubes. For an illuminating discussion of light collection in large volume scintillators the reader is directed to the work of Brini et al (BR55). In this paper, the authors discuss several topics including light output uniformity and time response uniformity in large scintillators and present recommendations for achieving maximum uniformity of scintillator response. These recommendations are directly applicable to the online neutron monitor and should be seriously considered before any attempt is made at improving the ONM.

4) Great care should be taken in the selection of new photomultiplier tubes. The present tubes are old and very noisy and the noise pulses large enough to require lower level discriminator levels of about 0.16 MeVee. This discriminator level represents 30 percent of the three quarter peak light output predicted by the Monte Carlo simulation for 2.45 MeV neutrons (see figure 3-2). A significant reduction in this discriminator level may result in the reduction of the lower level discriminator problems discussed in detail above.

5) Throughout the use of the ONM it was repeatedly observed that the ONM is sensitive to magnetic fields. The gain of the ONM was observed to drop by a factor of 5 when it was placed about a metre from a large permanent magnet (the permanent magnet was the yoke of an inoperational quadrupole electromagnet).

It is well known that the gain of a photomultiplier tube is sensitive to magnetic fields because such fields may alter the trajectory of the accelerated electrons, particularly in the crucial flight from the photocathode to the first dynode (LE87). Larger photomultiplier tubes such as the RCA 4522 are particularly susceptible to this problem because the electron flight paths tend to be long and thus the deflection due to magnetic fields more severe. Because the ONM will be required to operate in close proximity to a large electromagnet, an effort should be made to minimize the effect of magnetic fields upon the photomultiplier tube gain. This can be accomplished in three ways:

Photomultiplier tubes are currently available which are specifically designed to minimize the effects of magnetic fields. These tubes generally employ a short electron flight path from the photocathode to the first dynode and are known as 'Close Proximity Focusing' photomultiplier tubes. The second manner in which the effects of magnetic fields may be minimized is through some form of magnetic shielding. The simplest method of shielding is the use of mu-metal or iron to reduce the magnetic flux in the region of the photomultiplier tubes. The final technique to minimize magnetic effects is the optimum positioning of the ONM in the magnetic environment. It has been shown that the effect of magnetic fields upon photomultiplier tube gain is minimum when the axis of the tube is oriented along the magnetic field lines (LE87).

6) A recent modification has been made to the ONM in an attempt to minimize the lower level discrimination problems discussed in this section. In the system described in this work, the two photomultiplier tube pulses are fed into separate discriminators and separately digitized. In the new set up, the two pulses are added together using a resistive network to yield a sum pulse. The sum pulse is then split, one channel is sent to the 2249A ADC, the other channel to a lower level discriminator which provides a gate pulse for the ADC. Preliminary results show that this configuration appears to show less sensitivity to the position of the light producing event upon the ONM sum spectrum. This was tested by placing a small ^{60}Co source upon the ONM and observing the spectra at various source

positions along the scintillator. It is recommended that this sum technique be investigated as an alternative to the present dual discriminator method.

CHAPTER 5

Analysis of Deuterium Implantation Data

5.1 INTRODUCTION

In August of 1990, deuterium implantation runs were performed using the Narodny Ion Accelerator and the data system described in chapter one of this work. A twenty four hour implantation of palladium (Pd) and a seventeen hour implantation of titanium (Ti) were accomplished. A preliminary discussion of this work is given by McKee et al (MC91). The final chapter of this thesis is devoted to the analysis of the online neutron monitor data which was collected during the Pd and Ti implantation.

5.2 THE AUGUST 1990 DATA

The only identifiable feature present in a 1990 ONM background spectrum is the cosmic muon through peak which appears to the right of centre in figure 5-1(a). Although the ONM was also subjected to a ^{60}Co gamma ray source and a Ra-Be neutron source (a significant source of ^{214}Bi gamma rays), this data is not very useful because the ONM lower level discriminator was set so high that only

Figure 5-1

ONM spectra, August 1990.

(a) Background spectrum of Narodny room showing cosmic muon through peak centred at about channel 220.

(b) Spectrum accumulated during the entire 24 hour deuterium implantation of palladium showing the cosmic muon through peak and the anomalous structure discussed in the text.

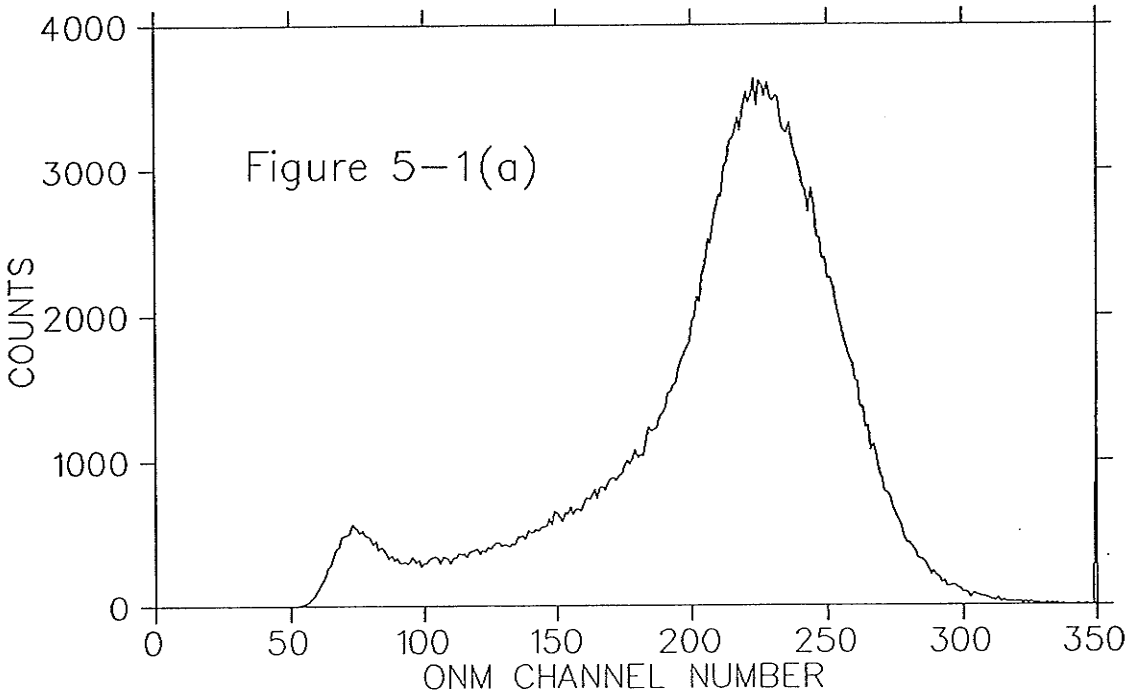
Figure 5-1(a)
COUNTS
4000
3000
2000
1000
0
0
50
100
150
200
250
300
350
ONM CHANNEL NUMBER

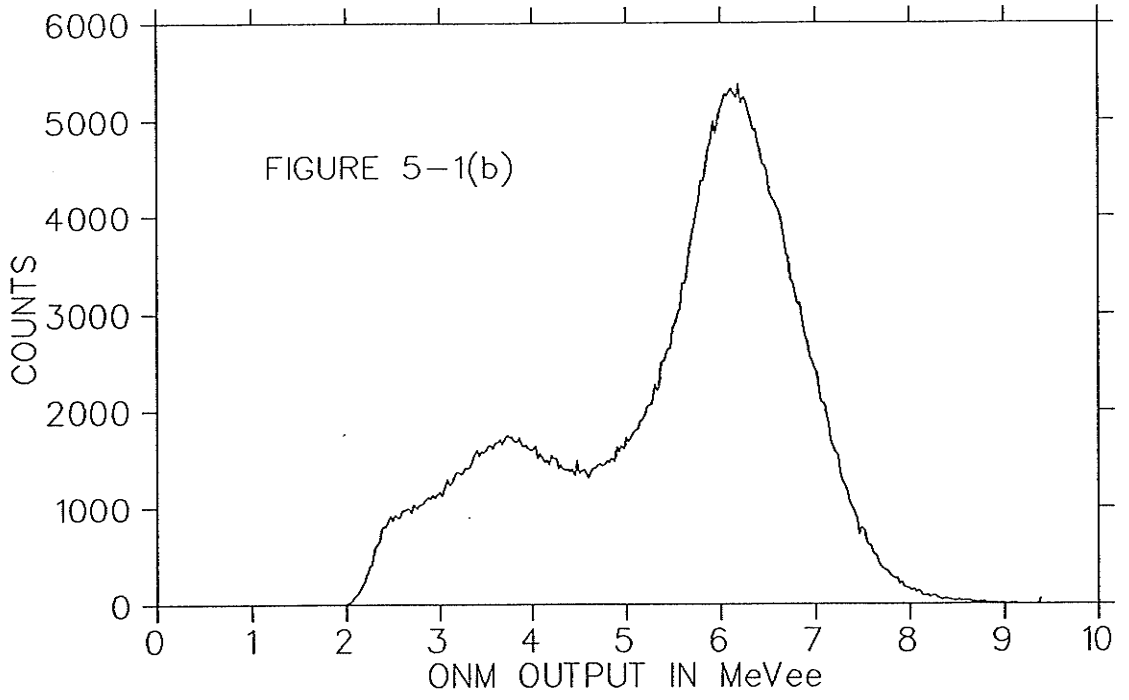
FIGURE 5-1(b)
COUNTS
6000
5000
4000
3000
2000
1000
0
0
1
2
3
4
5
6
7
8
9
10
ONM OUTPUT IN MeVee

the upper tail of the gamma ray spectra were visible.

The online neutron monitor is also an efficient detector of background radiation. A significant contribution to this background is from ^{40}K, which has a gamma ray at 1.5 MeV (PE89). Other environmental gamma rays which may be detected include those from ^{214}Bi (1.8, 2.1 and 2.2 MeV) and ^{81}Tl (2.6 MeV). In the summer of 1990, the detection of these environmental gamma rays was misinterpreted as random coincidences caused by noise in the ONM photomultiplier tubes and the lower level discriminators were set such that these events were eliminated from the ONM spectrum. In doing this it is possible that the lower level of the ONM was set at a light output greater than 2 MeVee.

Figure 5-1(b) shows the ONM spectrum obtained over the entire 24 hour Pd deuterium implantation run of August 1990. The structure to the left of the cosmic muon through peak is believed to be the result of nuclear processes which may be occurring in the Pd sample. During the first two hours of the implantation this anomalous structure was not evident in the ONM spectrum. As time progressed, the structure increased in size until about 10 hours into the run where the structure appeared to remain the same size for the remainder of the implantation.

In the Ti run a similar structure was apparent in the ONM spectrum throughout the 17 hour implantation. At the end of the Ti run, data was gathered with the

deuterium beam off and the anomalous structure was not evident in the ONM spectrum.

5.3 ONLINE NEUTRON MONITOR CALIBRATION

The only useful calibration information contained within the 1990 data is the position and width of the cosmic muon through peak. This data can be compared with the position and width of the cosmic muon through peak for the current ONM setting and a light output calibration of the 1990 ONM configuration may be inferred. The following scheme was employed.

1) A gaussian distribution was fitted to the lower side of the cosmic muon through peak of figure 5-1(b) in the same manner that a gaussian distribution was fitted to the cosmic muon through peak of chapter 2. This fit yielded a centroid at channel 220 and a standard deviation of 21.9.

2) The ratio of the standard deviation obtained in step 1. and the standard deviation of the cosmic muon through peak obtained in chapter 2 are related to the slope of the of the ONM light output calibration (see equation 2-1) in the following manner:

$$\sigma_1/\sigma_2 = m_2/m_1 \qquad \text{Equation 5-1}$$

Where $\sigma_{1(2)}$ is the standard deviation of the cosmic muon peak in figure 5-1(b) (figure 2-4) and $m_{1(2)}$ is the slope of the ONM calibration in figure 5-1(b) (figure 2-4).

3) Using equation 5-1(b) and the location of the cosmic muon peak in figure 5-1(b) the light output of the ONM in the 1990 configuration may be expressed as.

$$E(\text{MeVee}) = (M_2 \times \text{CHANNEL}) + C \qquad \text{Equation 5-2}$$

Where E is the light output in units of MeVee and:

$$M_2 = 0.0249 \text{ MeVee/CHANNEL}$$

$$C = 0.662 \text{ MeVee}$$

Equation 5-2 was used to express the horizontal axis of figure 5-1(b) in units of MeVee.

If the light output calibration given by equation 5-2 is accurate, it must be concluded that the lower level discriminator of the ONM in the 1990 configuration was set at a light output level of about 2.4 MeVee. A recent measurement of the ONM background spectrum showing both the cosmic muon structure and structure attributed to background gamma radiation is presented in figure 5-2. A comparison

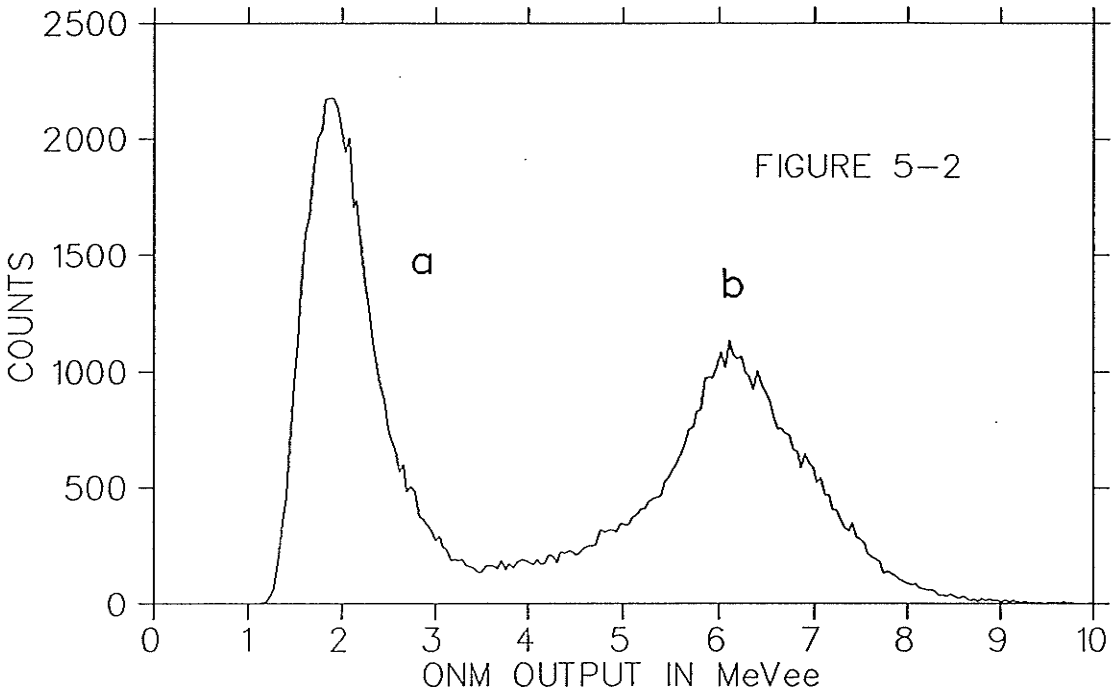

Figure 5-2

Recent ONM background spectrum taken in the cyclotron experimental area showing:

a) Structure believed to be the result of background gamma radiation.

b) The cosmic muon through peak.

of figures 5-2 and 5-1(a) suggests perhaps a lower level discriminator setting of about 2.8 MeVee would be more appropriate.

5.4 IDENTIFICATION OF THE ANOMALOUS STRUCTURE PRESENT IN THE AUGUST 1990 DATA

From the above calibration it is apparent that the anomalous structure present in the Pd implantation data is centred at a light output of about 4 MeVee. If this structure were due to n-p elastic scattering alone it would correspond to neutrons with energy in excess of 9 MeV (see figure 3-2). Because there is no reason to expect significant production of such high energy neutrons from the deuterium implantation process it is prudent to explore alternate explanations for the anomalous structure in figure 5-1(b).

Figure 5-3(a) presents a recent ONM background spectrum showing the cosmic muon peak. Figure 5-3(b) shows a recent ONM spectrum of the Am-Be neutron source. The Am-Be neutron source is also a source of 4.4 MeV gamma rays. The Am-Be source was situated in a cylindrical drum of wax which served to shield the ONM from fast neutrons but allow the passage of the gamma rays.

The structure to the left of the cosmic muon peak in figure 5-3(b) is believed to be the 4.2 MeV compton edge corresponding to the 4.4 MeV gamma ray. Comparing figures 5-1(a) and (b) with figures 5-3(a) and (b) it seems quite

Figure 5-3

Recent ONM spectra taken in the cyclotron experimental area.

(a) Background spectrum showing the cosmic muon through peak.

(b) Spectrum of the Am-Be neutron source showing the cosmic muon through peak and structure believed to be the Compton edge of the 4.44 MeV gamma ray.

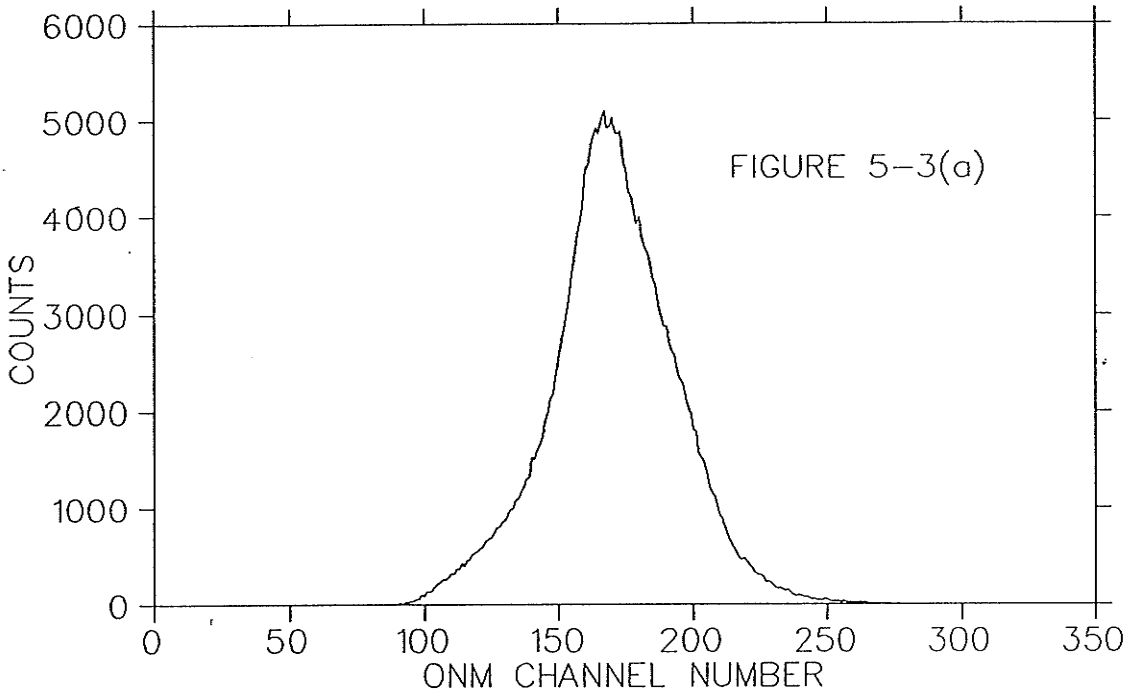

FIGURE 5-3(a)

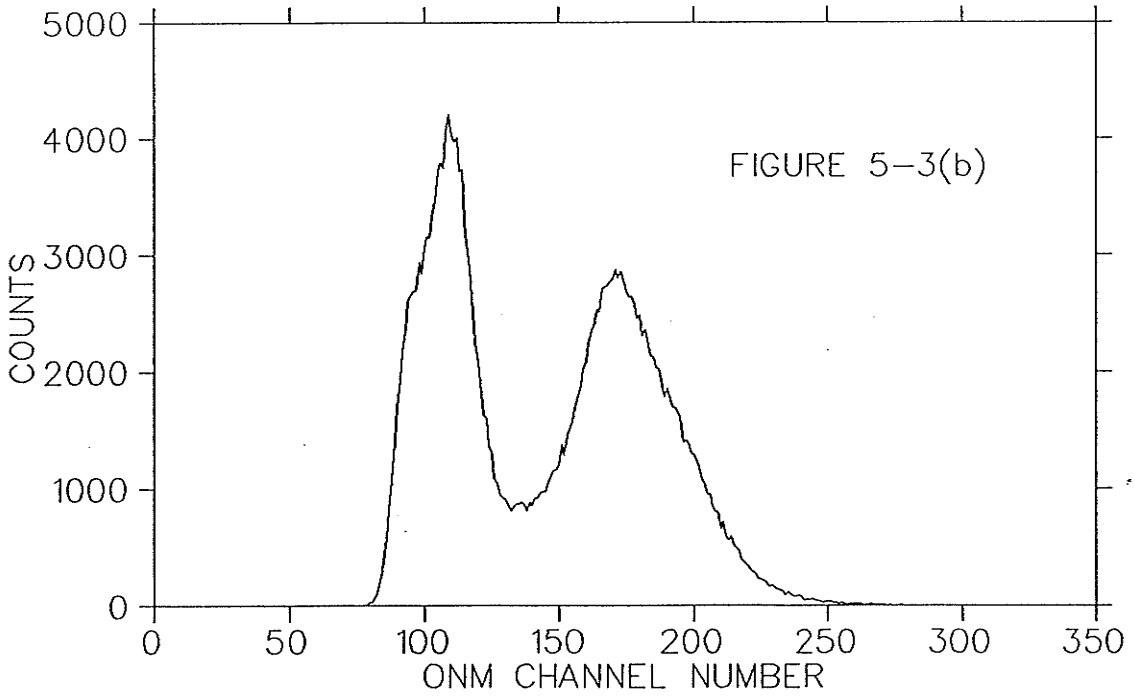

FIGURE 5-3(b)

plausible that the anomalous structure in the Pd implantation run may be the result of compton scattering of a gamma ray with energy of about 4 MeV. It is unclear however, whether such a gamma ray originates from processes occurring inside the scintillator or processes occurring in other materials within the Narodny room.

As discussed in chapter 2 of this work, the inelastic scattering of neutrons from ^{12}C in the scintillator may lead to the production of a 4.4 MeV gamma ray. This gamma ray may be subsequently detected in the ONM via the Compton scattering of electrons. The threshold neutron energy for this interaction is 4.7 MeV. Although it is possible that neutrons with energies in excess of 4.7 MeV are produced during the deuterium implantation (see reaction 1-3 in chapter 1) it is unlikely that such neutrons would be produced in sufficient quantity to account for the anomalous structure.

If there was a significant amount of ^{1}H present in the palladium sample before the deuterium implantation process, 5.5 MeV gamma rays would be expected via hydrogen-deuterium warm fusion (see reaction 1-5 in chapter 1). However, the anomalous structure was not observed in the ONM spectrum until the third hour of the implantation exercise and therefore it is unlikely that the anomalous structure can be attributed to the hydrogen-deuterium warm fusion reaction because such a reaction should have been evident as soon as the beam was turned on.

Another group of reactions which may be explored as the possible cause of the anomalous structure are those involving thermal neutron capture. Because the ONM contains a large amount of carbon the following reaction is of particular interest:

$$n + {}^{12}C \rightarrow {}^{13}C + 4.95\ MeV \qquad \text{Reaction 5-1}$$

This reaction is known to proceed via three channels, however only two channels occur with significant probability. (AJ91):

$$n + {}^{12}C \rightarrow {}^{13}C + \gamma(4.95\ MeV) \quad 67.47\% \qquad \text{Reaction 5-2}$$

$$n + {}^{12}C \rightarrow {}^{13}C^{*} + \gamma(1.26\ MeV) \quad 32.36\% \qquad \text{Reaction 5-3}$$

$${}^{13}C^{*} \rightarrow {}^{13}C + \gamma(3.68\ MeV)$$

The total absorption cross section is 3.5 mb for thermal neutrons.

The rate of neutron absorption per unit volume of plastic scintillator may be obtained via the following expression (CO78).

$$A = N\sigma\phi_n \qquad \text{Equation 5-3}$$

Where A is the rate of neutron absorption per unit volume, N is the number density of ^{12}C in the NE-102 scintillator (cm^{-3}), σ is the total absorption cross section and ϕ_n is the flux of thermal neutrons ($cm^{-2} \times s^{-1}$) in the vicinity of the ONM. The following values were used:

$$N = 4.74 \times 10^{22} \ cm^{-3}$$

$$\sigma = 0.0035 \times 10^{-24} \ cm^2$$

Substituting the appropriate constants and multiplying by the volume of the ONM scintillator (4795 cm^3) the rate of absorption in the ONM α , can be written:

$$\alpha = (0.79) \phi_n \qquad \text{Equation 5-4}$$

From the indium activation data (see chapter 1) the fast neutron production rate, averaged over the entire Pd deuterium implantation run was estimated to be 2500 neutrons per second. The thermal neutron flux in the Narodny room may be estimated with the following expression (PA73):

$$\phi_n = (1.25 \ Q) / \Sigma \qquad \text{Equation 5-5}$$

Where ϕ_n is the thermal neutron flux in the Narodny room , Q is the rate of fast neutron production and Σ is the surface area of the inside walls of the Narodny room in cm^2. Using the above equation, the average thermal neutron flux in the Narodny room during the Pd deuterium implantation is estimated to be 1.08×10^{-3} cm^{-2} s^{-1}. Substitution of this value into equation 5-4 yields a gamma ray production rate in the plastic scintillator of 8.5×10^{-4} s^{-1}.

During the Pd deuterium implantation exercise the anomalous structure corresponds to a counting rate of about one Hz. This counting rate is about four orders of magnitude greater than the counting rate expected from the neutron capture gamma rays of reaction 5-1 and therefore it is unlikely that this specific neutron capture reaction is responsible for the anomalous structure observed in the ONM spectrum.

A similar calculation was performed for thermal neutron capture in the copper sample holder. This calculation yielded a gamma ray production rate of about 10^{-3} photons per second and therefore it is likely that the anomalous structure cannot be attributed to neutron capture in the copper sample holder alone.

Another possible source of neutron capture gamma rays is the concrete walls which surround the Narodny accelerator. Studies of concrete subjected to a

flux of thermal neutrons reveal that gamma rays with energies between three and five MeV are a major constituent of the neutron capture gamma radiation spectrum (PR57). The greatest source of this gamma radiation (about 77%) is neutron capture by the silicon isotopes ^{28}Si, ^{29}Si and ^{30}Si. Silicon is also of interest because the cascade time from the capture state to the ground state is very short for all three isotopes and therefore the gamma emission rate is defined by the neutron absorption rate in a low thermal neutron flux environment.

An exact calculation of the intensity of the gamma radiation in the Narodny room caused by neutron capture in the walls would be difficult. However, it is possible to obtain an estimate of the photon intensity by making the following assumptions:

i) The Narodny room is a spherical void inside an infinite volume of concrete.

ii) The ONM neutron detector is a sphere located at the centre of the spherical void. The spherical ONM has the same surface area as the real cylindrical detector.

iii) Only gamma radiation originating from silicon and with energy between three and five MeV will be considered.

iv) All gamma radiation from the concrete will be assumed to originate from the surface of the spherical void.

All data regarding thermal neutron capture in concrete was obtained from table 6.6.3 of Price, Horton and Spinney (PR57). The table presents typical values for Portland concrete.

Let the radius of the ONM be r and the radius of the spherical void be R. The probability that a photon emitted at the surface of the void will pass through the ONM is given by the ratio of the solid angle subtended by the ONM (Ω) to the total solid angle available to the photon (Ω_t):

$$P = \Omega / \Omega_t$$

Where,

$$\Omega = 2\pi [1 - (1 + r^2 / R^2)^{-1/2}]$$

and

$$\Omega_t = 4\pi$$

Therefore,

$$P = [1 - (1 + r^2 / R^2)^{-1/2}] / 2 \qquad \text{Equation 5-6}$$

The thermal neutron flux at a depth z in the concrete wall ($\phi_c(z)$) may be expressed in terms of the thermal neutron flux at the surface of the void (ϕ_n) and the thermal diffusion length of concrete (Λ) (PR57).

$$\phi_c(z) = \phi_n \exp[-z/\Lambda] \qquad \text{Equation 5-7}$$

Where

$$\Lambda = 7.0 \text{ cm.}$$

A diffusion length of seven centimetres suggests that the thermal neutron flux in the concrete will only be significant less than about 20 centimetres from the surface. Therefore, the assumption that all absorption gamma rays originate from the concrete surface has some validity.

The photon production per second, per cm^{-3} at a depth z (i(z)) may be expressed in terms of the neutron flux at a depth z and the capture length λ.

$$i(z) = \phi_c(z) / \lambda \qquad \text{Equation 5-8}$$

Where

$$\lambda = 204 \text{ cm}$$

The rate of photon production within the concrete can now be estimated by integrating equation 5-8 over all the concrete. The integration over the solid angle is trivial and yields 4π. The radial integral may be expressed as:

$$\int_{R}^{\infty} \exp[\, -(y-R)/\Lambda \,]\, y^2\, dy$$

Where y is the radial distance from the cetre of the void.

Integration yields a total rate of photon production I_t.

$$I_t = 2\pi\, \phi_n\, (\Lambda/\lambda)\ \ [\, 2\Lambda^2 + 2\Lambda R + R^2 \,] \qquad \text{Equation 5-9}$$

The rate at which photons enter the ONM (I_{ONM}) may be expressed in terms of the total photon production rate (I_t) and the probability that a photon produced in the wall will pass through the ONM (P).

$$I_{ONM} = I_t\ P \qquad \text{Equation 5-10}$$

Substituting the appropriate numerical values into equation 5-10 (assuming the void has a radius of 480 cm), the detection rate of photons caused by neutron capture in the walls is estimated to be 0.016 photons per second. Although this

result is still at least two orders of magnitude less than the observed rate in the ONM during the palladium implantation run it suggests that thermal neutron capture gamma radiation may be a constiuent of the anomalous structure.

5.5 CONCLUSIONS

From data and arguements presented sections 5.2 and 5.3 it is evident that the anomalous structure present in the palladium and titanium data of 1990 corresponds to a light output of about 4 MeVee. If this structure corresponds to the detection of fast neutrons, neutrons in excess of 4.7 MeV would be required to produce the structure via carbon inelastic scattering and neutrons in excess of 9 MeV would be required to produce the structure via neutron-proton elastic scattering (see section 3.2). Although neutrons in excess of 4.7 MeV may be produced during the fusion process (see reaction 1-3) it is very unlikely that such neutrons are produced in any significant quantity. Therefore it may be concluded that the anomalous structure is probably not the result of the interaction of fast neutrons with the ONM scintillator.

An attempt was made to attribute the anomalous structure to capture gamma rays resulting from a thermal neutron flux in the Narodny room and the adjacent concrete walls. The calculation of capture gamma ray production in the ONM and the copper sample holder yielded results between 10^{-3} and 10^{-4} photons

per second. These results are clearly too small to account for the one Hz counting rate attributed to the anomalous stucture.

An estimate of the effect of neutron capture gamma rays originating in the concrete walls of the Narodny room was also made. The rate at which capture photons enter the ONM was estimated to be 0.033 photons per second. Although this rate is larger than that from neutron capture in the ONM or the copper sample holder, it is still not sufficient to fully account for the anomalous structure.

Although the exact cause of the anomalous structure is still elusive, the concrete calculation suggests that further investigation is warranted in the area of thermal neutron capture. It is suggested that in future deuterium implantation exercises an attempt is made to measure the gamma radiation spectrum in the Narodny room in the energy region of two to eight MeV. Such a measurement is crucial to the understanding of the ONM spectrum because the ONM is an efficient detector of gamma radiation and at the present time there is no way to differentiate between neutron and gamma events in the ONM spectrum.

Appendix

INTRODUCTION

This appendix contains the Turbo Pascal source codes for the data acquisition programs COLLECT and TOF. Both codes were designed using Turbo Pascal, Copyright Borland International 1987, 1988. The PC type microcomputer was interfaced with the CAMAC system using a Model 6002 crate controller an a Model PC004 interface card both manufactured by DSP Technology Incorporated of Fredmont California. The DSP Model 9100 software package was employed to support the use of Turbo Pascal.

A.1 The COLLECT Data Acquisition Program

The COLLECT program was developed in the summer of 1990 by John K. Mayer, Keith Furutani and the author. The program is discussed in detail in section 1.4 of this thesis.

```
{$N+}{$E+}{$M $4000,0,0}
program collect (input,output);

uses dos,crt,graph,glob;
{$I camturbo.v4}
label 10;


{************************************************************************}
{** PROCEDURE CLOSEUP - This procedure makes the closing logbook       **}
{**            entry and halts the program.                            **}
{************************************************************************}

procedure closeup;
     begin

     {**** Make logbook entry for end of run ****}

     n:=23; f:=0;
     for a := 0 to 4 do
          cami24(n,f,a,scalar[a],q,x);
     gettime(hour,minute,second,sec100);
     getdate(year,month,day,dayofweek);
     writeln(log,'RUN No. ',run_number,'  ended: ',day,'/',month,
                 '/',year,' ':3,hour:2,':',minute:2,':',second:2);
     writeln(log,scalar[0]:10,scalar[1]:10,scalar[2]:10,
                 scalar[3]:10,scalar[4]:10);
     writeln(log);
     close(log);
     halt;
     end;



{************************************************************************}
{** PROCEDURE DISPLAY_SCALARS - This procedure displays the running    **}
{**             scalars during the data taking.                        **}
{************************************************************************}

procedure display_scalars;


  begin
  gettime(hour,minute,second,sec100);
  clrscr;
  writeln(' ':30,' FUTILE SCALAR PAGE ');
  writeln(' ':30,' ******************');
  writeln;
  writeln('Beam Current',' ':12,'Time',' ':7,'Real Time');
  writeln('~~~~~~~~~~~~',' ':12,'~~~~',' ':7,'~~~~~~~~~');
  writeln(' ',scalar[0]:10,' ':7,scalar[1]:10,' ':7,
              hour:2,':',minute:2,':',second:2);
  writeln;
  if scalar[2] <> 0 then
       ONM_dead := (1 - (ONM_display/scalar[2]))*100.0
  else
       ONM_dead := 0.0;
  writeln('ONM Triggers',' ':6,'ONM Events');
  writeln('~~~~~~~~~~~~',' ':6,'~~~~~~~~~~');
  writeln(' ',scalar[2]:10,' ':7,ONM_display:10);
  writeln;
  if scalar[3] <> 0 then
       Ge_dead := (1 - (Ge_display/scalar[3]))*100.0
  else
       Ge_dead := 0.0;
  writeln(' Ge Triggers',' ':7,'Ge Events',' ':7,'Ge Busy-outs ');
  writeln(' ~~~~~~~~~~~~',' ':7,'~~~~~~~~~',' ':7,'~~~~~~~~~~~~ ');
```

```
  writeln(' ',scalar[3]:10,' ':7,Ge_display:10,' ':9,
             scalar[4]:10);
  writeln;
  writeln('Current RUN Number :',run_number:3,' ':20,
          'ONM Dead Time (%): ',ONM_dead:8:1);
  writeln('Current Sub_RUN No.:',subrun_number:3,' ':20,
          'Ge Dead Time (%):  ',Ge_dead:8:1);
  writeln(' ':20,'Bytes Transferred :',packet*512:9);
  writeln;
  writeln('ALT - D : Dump data to Vax');
  writeln('ALT - Q : Dump data to Vax and quit');
  writeln('ALT - K : Kill the program without a dump');
  writeln('ALT - S : Display scalars');
  end;


{*************************************************************************}
{** PROCEDURE DUMP2VAX - This procedure dumps the acquired data from    }
{**              the hard drive to the VAX via a DOS call to FTP.       }
{*************************************************************************}

     procedure dump2vax;

     begin
     rewrite(trans);
     writeln(trans,'echo off');
     writeln(trans,'stackey !');
     write(trans,'stackey "futile"CR"blue_indigo"CR"bput e:\data\run.dat ');
     write(trans,'fusion',run_number,'.',subrun_number,'"');
     writeln(trans,'CR"close"CR"quit"CR');
     writeln(trans,'ftp 130.179.17.12');
     close(trans);
     writeln('**** DUMPING BUFFER TO VAX ****');
     swapvectors;
     exec('c:\command.com',' /c e:\fusion\send2vax.bat');
     swapvectors;
     if doserror <> 0 then
          writeln('*** DOS ERROR !!!!!   ',doserror)
     else
          writeln('#### SUCCESSFUL TRANSFER ####');
     display_scalars;
     end;


{*************************************************************************}
{** PROCEDURE EVENT_BUILDER - This procedure formats the CAMAC data     }
{**             and initiates the dumping of the data to the VAX at     }
{**             appropriate times.                                      }
{*************************************************************************}

     procedure event_builder;

     begin
     data[index+1] := Ge_data;
     data[index+2] := ONM_data[0];
     data[index+3] := ONM_data[1];
     index := index + 3;
     if index-3 = 123 then
          begin
          n:=23; f:=0;
```

```
        for a := 0 to 4 do
             begin
             cami24(n,f,a,scalar[a],q,x);
             data[124+a] := scalar[a];
             end;
        count := 128;
        {blockwrite(hard_disk,data,count,result);}
        packet := packet + 1;
        ONM_display := ONM_events;
        Ge_display := Ge_events;
        index := 0;
        if dump_file then
            begin
            close(hard_disk);
            dump2VAX;
            getdate(year,month,day,dayofweek);
            gettime(hour,minute,second,sec100);
            writeln(log,'RUN No. ',run_number,'.',subrun_number,
                    '  dumped: ',day,'/',month,'/',year,' ':3,hour:2,':',
                   minute:2,':',second:2);
            dump_file := false;
            rewrite(hard_disk,4);
            subrun_number := subrun_number + 1;
            packet := 0;
            end;
        if dump_file_quit then
            begin
            close(hard_disk);
            dump2VAX;
            closeup;
            end;
        end;
    end;


{*********************************************************************}
{** PROCEDURE EXTRACT_DATA - This procedure is called when a CAMAC   }
{**             LAM is detected by the caml routine. It tests to see }
{**             which module generated the LAM, extracts the data,   }
{**             histograms it, and calls the procedure for formatting}
{**             the output to disk.                                  }
{*********************************************************************}

    procedure extract_data;

    begin
    GE_data     := 9999;          {Initialize dummy data values}
    ONM_data[0] := 9999;
    ONM_data[1] := 9999;
    LAM_ONM := false;
    LAM_Ge  := false;

    {**** Determine if Ge detector is generating LAM ****}

    n:=8; a:=0; f:=8; q:=0;
    camo(n,f,a,null16,q,x);
    if q = 1 then
        LAM_Ge := true;
```

```
     {**** Determine if ONM detector is generating LAM ****}

     n:=10; a:=0; f:=8; q:=0;
     camo(n,f,a,null16,q,x);
     if q = 1 then
          LAM_ONM := true;

     {**** Extract Ge data and histogram ****}

     if LAM_Ge then
          begin
          n:=8; a:=0; f:=0;
          cami24(n,f,a,Ge_data,q,x);
          Ge_data := Ge_data - 1024;
          f:=9;
          camo(n,f,a,null16,q,x);
          Ge_events := Ge_events + 1;
          end;

     {**** Extract ONM data and histogram ****}

     if LAM_ONM then
          begin
          n:=10; f:=0;
          for a := 0 to 1 do
               cami24(n,f,a,ONM_data[a],q,x);
          ONM_events := ONM_events + 1;
          end;

     {**** Format data for storage and output ****}

     event_builder;
     end;


{************************************************************************}
{** PROCEDURE CLEAR - This procedure clears the LAM's of the 2249A     }
{**             and the 3511.                                          }
{************************************************************************}

procedure clear;
     begin
     n:=10; a:=0; f:=9;
     camo(n,f,a,null16,q,x);                  {Clear LAM of 2249A}
     n:=8; a:=0; f:=10;
     camo(n,f,a,null16,q,x);                  {Clear LAM of 3511}
     end;


{************************************************************************}
{** PROCEDURE LAMHANDLER - This procedure is invoked whenever the      }
{**             LAM asserted by a CAMAC module generates a non-zero    }
{**             CAML return.                                           }
{************************************************************************}

procedure LAMHandler;
     begin
     extract_data;          {Go get data from ADC(s)}
     clear;
     end;
```

```
{*********************************************************************}
{** PROCEDURE INITIALIZE - This procedure initializes the CAMAC crate}
{**            and the LAM capabilities of the ADC's used in the    }
{**            experiment. It also initializes the run variables.   }
{*********************************************************************}

procedure initialize;

     begin
     clrscr;
     writeln('    ************************************************');
     writeln('           BEGINNING DATA AQUISITION NOW !!!!       ');
     writeln('    ************************************************');
     writeln;
     writeln(' Enter a UNIQUE RUN NUMBER (one never used previously)');
     writeln;
     write('STARTING RUN NUMBER ==> ');
     read(run_number);
     subrun_number := 1;

     assign(hard_disk,'e:\data\run.dat');
     assign(log,'e:\data\logbook.txt');
     assign(trans,'e:\fusion\send2vax.bat');
     rewrite(hard_disk,4);
     append(log);

     packet := 0;
     Ge_display := 0;
     ONM_display := 0;
     index := 0;
     null24 := 0;
     null16 := 0;
     dump_file := false;
     dump_file_quit := false;
     for b := 0 to 4 do
          scalar[b] := 0;
     Ge_events := 0;
     ONM_events := 0;


{***** Setup and clear the CAMAC hardware now *****}

     f:=1; crate_set(f);              {Set PC board to crate 1}
     f:=64; camcl(f);                 {Clear the crate}

     n:=23; a:=0; f:=24; null24:=0;
     camo24(n,f,a,null24,q,x);        {Disable LAM of 3610 scalar}
     f:=9;
     for a := 0 to 4 do
          camo24(n,f,a,null24,q,x);   {Clear 3610 channels 0 - 4}

     n:=10; a:=0; f:=9; null16:=0;
     camo(n,f,a,null16,q,x);          {Clear module and LAM of 2249}
     f:=26;
     camo(n,f,a,null16,q,x);          {Enable LAM}

     n:=8; a:= 0; f:=24; null16:=0;
     camo(n,f,a,null16,q,x);          {Disable LAM of 3511}
     f:=10;
     camo(n,f,a,null16,q,x);          {Clear LAM}
     f:=16; data16:=1028;
     camo(n,f,a,data16,q,x);          {Write gain and offset}
     f:=26;
     camo(n,f,a,null16,q,x);          {Enable LAM of 3511}

     end;
```

```
{*************************************************************************}
{** MAIN PROGRAM                                                         *)
{*************************************************************************}

begin
initialize;
clear;

{**** Make logbook entry for start of run ****}

n:=23; f:=0;
for a := 0 to 4 do
     cami24(n,f,a,scalar[a],q,x);
gettime(hour,minute,second,sec100);
getdate(year,month,day,dayofweek);
writeln(log,'RUN No. ',run_number,'  started: ',day,'/',month,'/',year,' ':3,
            hour:2,':',minute:2,':',second:2);
writeln(log,scalar[0]:10,scalar[1]:10,scalar[2]:10,
           scalar[3]:10,scalar[4]:10);

display_scalars;

10: LAM := 0;
    caml(LAM);
    if LAM <> 0 then
        LAMHandler;

    if keypressed then
        begin
        control := readkey;
        if control = #032 then
             dump_file := true;
        if control = #016 then
             dump_file_quit := true;
        if control = #037 then
             begin
             close(hard_disk);
             closeup;
             end;
        if control = #031 then
             display_scalars;
        end;
   goto 10;
end.
```

A.2 The TOF Data Acquisition Program

The TOF program was developed to control the data acquisition process for the Compton scattering measurement (see chapter two of this work) and for the neutron time of flight measurement (see chapter four of this work). The program is discussed in detail in section 4.5 of this thesis.

```
{$N+}{$E+}
program tof (input,output);
uses crt,dos,histplot,globals1;

{$I camturbo.v4}
label 30,40,50,60,70,100,707;

var
     {variables for data aquisition system}
     flag,i,a,d1,d2,tdc,nai,f,n,q,x,m,ians,ians2,dummy,dummy2:integer;
     dd1,dd2,dds,c,cc,num1,nnai,nonm,rtime,ai,onm,ime:longint;
     disk,diskh : text;
     control: string[1];
     answer:char;
     hist1,hist2,hists,time,gamma:one_dim;

{initiate variables and CAMAC hardware}
begin
   707:
   clrscr;writeln;writeln;
   writeln('  Welcome to the Neutron Time of Flight Data Program');
   writeln;writeln;
   writeln('  Data will be logged as neut.evt');writeln;
   writeln('  Histograms will be dumped as neut.his');writeln;

   assign(disk,'e:\data\neut.evt');
   rewrite(disk);
   for i:= 0 to 1400 do
     begin
      hist1[i]:=0;
      hist2[i]:=0;
      hists[i]:=0;
      time[i]:=0;
      gamma[i]:=0;
     end;
  d1:=0;d2:=0;tdc:=0;nnai:=0;nonm:=0;rtime:=0;
  ime:=0;ai:=0;onm:=0;c:=0;cc:=0;
  f:=1;
  crate(f);
  f:=64;
  camcl(f);                    {clear crate}
  n:=9;f:=26;a:=0;
  camo(n,f,a,d1,q,x);          {enable 3511 LAM}
  f:=10;
  camo(n,f,a,d1,q,x);          {clear 3511 and LAM}
  n:=9;f:=16;nai:=1028;
  camo(n,f,a,nai,q,x);
  for n:=10 to 11 do           {enable and clear 2249 adc and 2228 tdc}
    begin
     f:=26;                    {enable LAM of module}
     camo(n,f,a,d1,q,x);
     f:=9;                     {clear LAM and module}
     camo(n,f,a,d1,q,x);
    end;

  30:
  cc:=cc+c;                    {cc=total number of events digitized}

                               {c=number of events digitized in one evocation}
                               {of the main data collection process}
                               {ie c=num1 after an evocation}
  writeln;
  write('          Enter number of data values.   ');
  readln(num1);
  write('          Data on screen, Yes 1 / No 0   ');
  readln(ians);
  writeln;
```

```
writeln('          <ALT-N> number of counts in buffer.');
writeln('          <ALT-D> display spectra.');
writeln('          <ALT-Q> quit data collection.');writeln;
n:=17;f:=24;
camo24(n,f,a,nonm,q,x);     {disable scaler LAM}
f:=9;
for a:=0 to 5 do            {clear scaler}
    camo24(n,f,a,nonm,q,x);
c:=0;
while c<num1 do             {main data collection loop}
 begin                      {c is the number of valid events digitized}

  if keypressed then
     begin
     control:= readkey;
     if control = #049 then
       begin
         writeln('                Have ',c,' events in buffer.');
       end;
     if control = #032 then
       goto 40;
     if control = #016 then
       goto 60;
     end;

  q:=0;f:=8;n:=11;          {set n for tdc}

  while q=0 do
   begin
    camo(n,f,a,d1,q,x);
   end;                     {keep checking tdc for q=1 which signifies LAM}
                            {q=1 tells us that the tdc has taken in data and
                            is ready to transfer it}

  f:=0;a:=0;
  cami(n,f,a,tdc,q,x);              {read 2228 tdc}

  if tdc>1400 then goto 100;        {check for 2228 tdc overflow}

  n:=10;                            {set n for 2249 adc}

  cami(n,f,a,d1,q,x);               {aquire data from channel 0 of the}
                                    {2249 adc}

  if d1>1380 then goto 100;         {check if channel 0 of the 2249}
                                    {adc has overflown}

  a:=1;                             {repeat for channel 1 of the 2249}
  cami(n,f,a,d2,q,x);
  if d2>1380 then goto 100;

  n:=9;a:=0;                        {set n for 3511 adc}
  cami(n,f,a,nai,q,x);              {aquire data from 3511 adc}
  nai:=nai-1024;                    {correct for offset}

  writeln(disk,d1,'   ',d2,'  ',nai,'   ',tdc);   {write data to disk}
  if ians=1 then
       writeln(d1,'  ',d2,'  ',nai,'  ',tdc);    {write data to screen}

  dds:=round((d1+d2)/2);            {process data for histograms}
  hist1[d1]:=hist1[d1]+1;
  time[tdc]:=time[tdc]+1;
  hist2[d2]:=hist2[d2]+1;
  hists[dds]:=hists[dds]+1;
```

```
  if nai<1024 then
     gamma[nai]:=gamma[nai]+1;

  c:=c+1;

  100:                                  {reset CAMAC hardware}
  f:=9;
  for n:=10 to 11 do
      camo(n,f,a,d1,q,x);               {clear 2249 adc tdc and their LAMs}
  f:=10;n:=9;
  camo(n,f,a,d1,q,x);                   {clear 3511 and LAM}
 end;                                   {end of main data collection loop}

40:
ai:=0;onm:=0;ime:=0;                    {zero scaler variables}
n:=17;f:=0;a:=0;                        {read scaler}
cami24(n,f,a,ai,q,x);    {ai=number of events detected by const. frac. disc.}
a:=1;
cami24(n,f,a,onm,q,x);   {onm=number of events detected by AND gate}
a:=2;
cami24(n,f,a,ime,q,x);   {count generated by pulser and divide by 100 scaler}
nnai:=nnai+ai;nonm:=nonm+onm;rtime:=rtime+ime;  {record scalers}
close(disk);

70:                          {data viewing}
writeln;
writeln('  We have ',nnai,' gamma events and ',nonm,' ONM events');
writeln;writeln;
writeln('  The run time is ',rtime);writeln;writeln;
writeln('  We have ',c,' coincidences');writeln;writeln;
writeln;
write(' Spectrum desired = (ONM 1 or 2, 3 for ONM sum, 4 for time');
write(' or 5 for Gamma) ');
readln(flag);
if (flag<1) or (flag>5) then
    goto 70;

  if flag=1 then
     display_histogram(flag,hist1);
  if flag=2 then
     display_histogram(flag,hist2);
  if flag=3 then
     display_histogram(flag,hists);
  if flag=4 then
     display_histogram(flag,time);
  if flag=5 then
     display_histogram(flag,gamma);


50:                          {options}
writeln;writeln;writeln;
write('Get more data 0 / Quit 1 / Plot data 2 / Reset 3     ');
readln(x); writeln;

{note that if 0 is selected program will crash}
{if 3 is selected all data will be lost and data collection will commence}
{selection of 1 will ensure that all data is saved}

  if x=2 then                {graph more data}
  goto 70;

if x= 0 then goto 30;        {get more data, at present program will crash}
```

```
if x= 3 then goto 707;      {reset}

60:                                  {quitting the program}
assign(diskh,'e:\data\nhist.dat');
rewrite(diskh);
writeln('Writing spectra to disk...Good bye....');
writeln(diskh,nnai,'  ',nonm,'  ',c,'  ',rtime);   {saving scaler values}
writeln(diskh);writeln(diskh);
for i:= 1 to 1400 do
  begin                      {saving histograms}
    writeln(diskh,hists[i],'  ',hist1[i],'  ',hist2[i],'  ',gamma[i]);
  end;
close(diskh);
end.
```

REFERENCES:

(AJ91) F. Ajzenberg-Selove, Nucl. Phys. A523 (1991) 1.

(BA91) A. Baldini, C. Bemporad, F. Cei, G. Giannini, P. Razzi and M.Grassi, Nucl. Instr. and Meth. A305 (1991) 475.

(BE48) P.R. Bell, Phys. Rev. 73 (1948) 1405.

(BI51) J.B. Birks, Proc. Phys. Soc. A64 (1951) 874.

(BI64) J.B. Birks, The Theory and Practice of Scintillation Counting (Pergamon Press, London 1964).

(BR55) D. Brini, L. Peli, O. Rimondi and P. Veronisi, Nuovo Cimento, Supplemento Al Volume II , Serie X Del Nuovo Cimento (1955) 1048.

(BR59) F.D. Brooks, Nucl. Instr. and Meth. 4 (1959) 151.

(BR79) F.D. Brooks, Nucl. Instr. and Meth. 162 (1979) 477.

(BR86) Edgardo Browne and Richard B. Firestone, Table of Radioactive Isotopes. ed. Virginia S. Shirley (John Wiley and Sons, New York 1986).

(CE79) R.A. Cecil, B.D. Anderson and R.Madey, Nucl. Instr. and Meth. 161 (1979) 439.

(CO78) Thomas J. Connolly, Foundations of Nuclear Engineering (John Wiley and Sons, New York 1978).

(CO89) Paulo R.P. Coelho, Aucyone A. Da Silva and Jose R. Maiorino, Nucl. Instr. and Meth. A280 (1989) 270.

(CR70) R.L. Craun and D.L. Smith, Nucl. Instr. and Meth. 80 (1970) 239.

(CZ64) J.B. Czirr, D.R. Nygren and C.D. Zafiratos, Nucl. Instr. and Meth. 31 (1964) 226.

(DI54) D.E. Diller and M.F. Crouch, Phys. Rev. 93 (1954) 362.

(DU89) J.J.G. Durocher, D.M. Gallop, C.B. Kwok, M.S. Mathur, J.K. Mayer, J.S.C. McKee, A. Mirzai, G.R. Smith, Y.H. Yeo, K.S. Sharma and G. Williams, Can. J. Phys. 67 (1989) 624.

(FI90) V.V. Filchenkov, A.D. Konin and A.I. Rudenko, Nucl. Instr. and Meth. A294 (1990) 504.

(FO80) J.L. Fowler, J.A. Cookson, M. Hussain, R.B. Schwartz, M.T. Swinhoe, C. Wise and C.A. Uttley, Nucl. Instr. and Meth. 175 (1980) 449.

(GA89) M. Gai, S.L. Rugari, R.H. France, B.J. Lund, Z. Zhao, A.J. Davenport, H.S. Isaacs and K.G. Lynn, Nature 340 (1989) 29.

(HA60) A.O. Hanson, Fast Neutron Physics Part I, ed. J.B. Marion and J.L. Fowler (Interscience, New York 1960).

(HA79) J.A. Harvey and N.W. Hill, Nucl. Instr. and Meth. 162 (1979) 507.

(JA56) D.B. James, G.A. Jones and D.H. Wilkinson, Phil. Mag. 1 (1956) 949.

(KA86) B.K. Kamboj and M.G. Shahani, Nucl. Instr. and Meth. A244 (1986) 513.

(KN89) Glenn F. Knoll, Radiation Detection and Measurement, second edition (John Wiley and Sons, New York 1989).

(LE87) William R. Leo, Techniques for Nuclear and Particle Physics Experiments (Springer-Verlag, Berlin 1987).

(MA78) Richard Madey, F.M. Waterman, A.R. Baldwin, J.N. Knudson, J.D. Carlson and J. Rapaport, Nucl. Instr. and Meth. 151 (1978) 445.

(MC91) J.S.C. McKee, G.R. Smith, J.J.G. Durocher, K. Furutani, C.B. Kwok, H.L. Johnston, M.S. Mathur, J.K. Mayer, A. Mirzai, Y.H. Yeo, K.S. Sharma and G. Williams, Anomalous Nuclear Effects in Deuterium/Solid Systems, A.I.P. Conference Proceedings 228, ed. Steven E. Jones, Franco Scaramuzzi and David Worledge (American Institute of Physics, New York 1991).

(PA73) H. Wade Patterson and Ralph H. Thomas, Accelerator Health Physics (Academic Press, New York 1973).

(PE89) R.D. Petrasso, X. Chen, K.W. Wenzel, R.R. Parker, C.K. Li and C. Fiore, Nature 339 (1989) 183.

(PR57) B.T. Price, C.C. Horton and K.T. Spinney, Radiation Shielding (Pergamon Press, New York 1957).

(RA80) W.D. Ramsay, Ph.D. Thesis, University of Manitoba (1980) unpublished.

(RA91) W.D. Ramsay TRIUMF, private communication, 1991.

(RU56) O.J.C. Runnals and R.R Boucher, Can. J. Phys. 34 (1956) 949.

(SE77) Emilio Segre, Nuclei and Particles, second edition (Benjamin/Cummins, Menlo Park California 1977).

(ST71) N.R. Stanton, Ohio State University High Energy Physics Laboratory Report C00-1545-92 (February, 1971).

(SW60) C.D. Swartz and G.E. Owen, Fast Neutron Physics Part I, ed. J.B. Marion and J.L. Fowler (Interscience, New York 1960).

(VI73) A.D. Vijaya and Arun Kumar, Nucl. Instr. and Meth. 111 (1973) 435.

(YE89) Y.H. Yeo, M.Sc. Thesis, University of Manitoba (1989) unpublished.

(ZE86) ZEUS Collaboration, The ZEUS Detector Technical Proposal (1986).